A review on Graphene Polymer Nanocomposites in Harsh Operating Conditions

Premika Govindaraj[a], Bronwyn Fox[a], Phillip Aitchison[b], Nishar Hameed[a*]

[a] Factory of the Future, Swinburne University of Technology, VIC 3127, Australia.

[b] Imagine Intelligent Materials, NSW 2018, Australia

Abstract

Development of high-performance composites operating in harsh conditions is gaining tremendous attention due to their broad range of applications such as mass transport, defense, energy, manufacturing, electronics, healthcare, and so forth. Some of the current challenges include the development of lightweight composites suitable for high or low temperatures, high impacts, and corrosive or radiation environments. Among various nanomaterials, graphene based materials have emerged as the most popular class of nanoadditive which can revolutionize every industry sectors. Herein, we briefly discuss the properties of graphene as a potential additive for high-performance composites. The review focuses on the functional properties of graphene based polymer nanocomposites in range of harsh operational conditions, such as cryo-mechanical properties, ballistic impact resistance, thermal conductivity, deicing/anti-icing behavior, self-cleaning, sensing properties and flame retardant properties. Finally, we conclude with an outlook for the development of graphene based polymer nanocomposites for harsh conditions by deliberating the major progress, challenges, and opportunities.

Keywords: Composites, graphene, mechanical, thermal, ballistic impact, cryogenic, deicing, anti-icing, self-cleaning, sensing

[*]*Corresponding author email –* nisharhameed@swin.edu.au

Table of Contents

1. Introduction

Materials operating in harsh conditions experience extremes in stress, strain, pressure, temperature, chemical reactivity, radiations, electric and magnetic fields[1-3]. Materials are central to every present and future technologies and they perform in range of applications. Some of the key operations includes: airplane fuselages and wind turbine housings are operated at high temperatures and in oxidative environment[4,5]; structural and cladding materials in nuclear reactors are subjected to radiation and corrosion[6]; electrodes in batteries and fuel cells experience large electrochemical forces and mechanical stress[7] underwater marine and civil structures are subjected to large loads[8]; and many more. Choice of materials in these operating condition plays a vital role. For example, composite cryo-tank which weighs 30% less and costs 25% less than the aluminum-lithium cryotanks can allow mass transport of 1,400 kg additional payload to low-earth orbit and beyond[9]. Thus, understanding and tailoring the performance of materials is fundamental. Further, the aging process of the materials is accelerated during their operational conditions, leading to reduced performance and eventually failure. Therefore, it is essential to consider the engineering requirements of materials in harsh operational conditions to allow them to be specifically tailored for their applications.

The use of polymers is increasing throughout many industries owing to their light weight and chemical resistance, which provides advantages over metals. Their versatility has allowed them to be used in harsh conditions, as components in aerospace, explosive, heavy machinery and submarine where they are subjected to extreme levels of strain rate, pressure, temperature and radiation[10]. By reinforcing polymers, their properties are enhanced and the resulting composites exhibit improved properties over a wide range of conditions. These polymer composites can be tailored for specific applications by appropriate selection of materials and processing techniques. Some of the major performance improvements of high-performance polymer composites are highlighted below.

The conventional polymer composites are usually reinforced with additives in the form of particulates, laminates or fillers to combine the strength of individual constituents and to improve the physical properties. For instance, the carbon fiber reinforced thermoplastic polyimide composites exhibited fiber direction tensile strength as high as 1200 MPa and operating on a temperature scale of -50 ^{o}C to 250 ^{o}C [11]. Similarly, glass fiber reinforced polymer composites retained 54%, 11% and 5% of the ambient temperature tensile, shear and compressive strengths respectively at 220 ^{o}C [12]. Although the discrete fillers in conventional composites result in modest improvement in mechanical strengths, they still suffer from reduced compliance and catastrophic failures due to poor interfacial bonding and dissimilarity in the coefficient of thermal expansion (CTE)[13].

On the other hand, composites reinforced with nanoadditives have developed over the past decade as the prospective class of materials. These nanocomposites exhibit better compliance and endurance compared to the conventional composites owing to the increased interfacial area and better interactions[14]. Currently, nanocomposites are reinforced with inorganic nanoparticles[15-17,18], metal nanoparticles[19,20], nanofibers[21-23] and carbon-based materials[24-27]. Most commonly used inorganic nanoparticles such as clay nanoparticles (eg. Montmorillonite, MMT) and ceramic particles exhibit improved strength, stiffness, thermal stability, optical transparency, flame retardancy and barrier properties[28,29]. For instance, an artificial columnar nacre-like microstructure was developed using MMT/hydroxyethyl cellulose exhibit tensile strength comparable to natural nacre (135 MPa) with excellent superoleophobicity (156.8^{o}), chemical stability and resistance to sand grain impingement[30]. In fact, clay-polymer nanocomposites have found their commercial application as timing belt covers for Toyota cars[31], as structural seat backs in Honda Acura[32] as well as functions as barrier resistance liners for fuel system components and beverages[33]. However, these stiff inorganic fillers compromise flexibility and biodegradability. Metal nanoparticles such as iron oxide, nickel, cobalt, copper, gold and silver nanoparticles also exhibit enhanced reinforcing properties by improving the electrical conductivity[34], magnetic properties[35], catalytic properties[36], plasmonic characteristics[37] and electromagnetic shielding effectiveness[38].

In recent times, structured carbon based materials such as fullerene and carbon nanotubes have emerged as more common nanostructures in high-performance composites[39]. Multi-walled carbon nanotubes reinforced elastomer composite with a cellular alignment of nanotubes performs as a durable O-rings for excavating deep oil resources [40]. These nanotubes based rubber O-rings show no leakage when exposed to a temperature of 260 ^{o}C and pressures as high as 239 MPa for 14 h. Although carbon nanotubes are regarded as promising nanoadditive owing to their properties, there are still some critical concerns which need to be addressed such as poor dispersibility, excessive aggregation, low interfacial interactions and poor control over surface chemistries.

Finally, various graphene materials have newly developed as a potential additive for advanced nanocomposites, can revolutionize numerous industrial sectors[41,42]. In this review, we are focussing on the graphene properties which make it as a prospective filler for harsh operational conditions. In the later session, we discuss the properties of graphene- polymer composites which are capable of functioning in harsh operational conditions. Furthermore,

the review in short detail also discusses the major challenges and opportunities of graphene-polymer nanocomposites with their potential applications.

1.1 Graphene - a prospective additive

In 2004, the isolation of graphene by Andre Geim and Kostya Novoselov bought revolutionary changes to several industries including the composite industry. Graphene is a single layer of covalently bonded carbon atoms organized in a hexagonal array. This two-dimensional material is the building block for many allotropes of carbon ranging from three-dimensional graphite (a stack of graphene sheets), to one-dimensional carbon nanotubes (a seamless graphene cylinder) to zero-dimensional buckyballs (a closed graphitic cage)[43,44]. The incredible properties and attractive architecture of graphene in a macroscopic scale have steered to the development of graphene reinforced polymer composites to have outstanding performances. Figure 1 depicts a scheme of suitable applications of graphene composites in modern day life for harsh operating conditions.

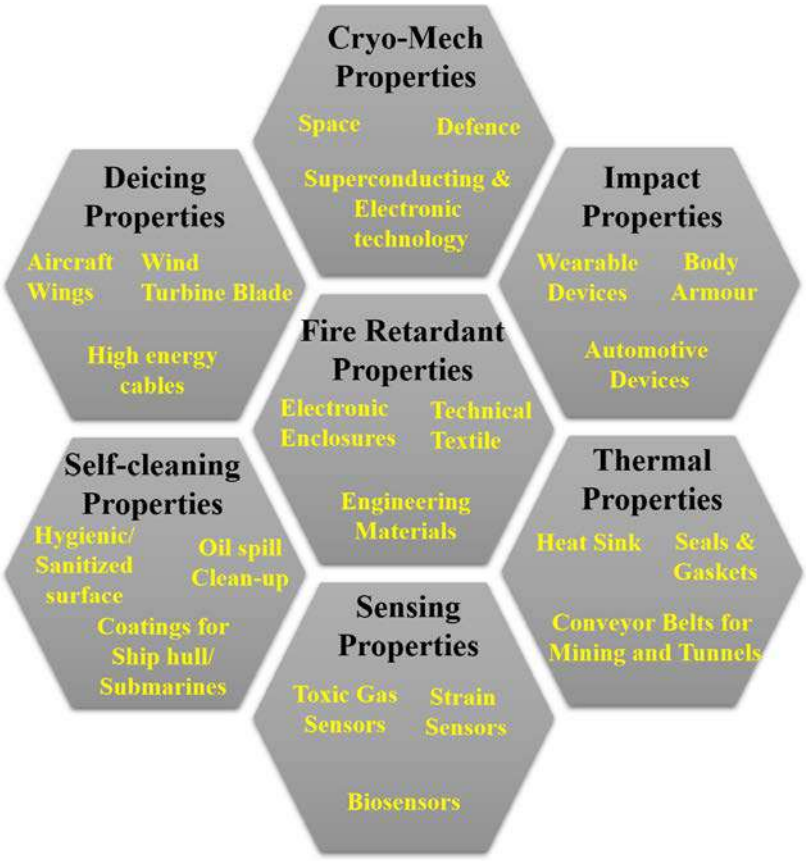

Figure 1. Scheme depicting various current and prospective applications of graphene-polymer composites for harsh operating conditions.

1.1.1. Properties of Graphene

Graphene can be considered as a prospective material for harsh operating conditions owing to their exceptional mechanical, electrical and thermal characteristics. For instance, graphene possesses the highest intrinsic electron mobility known which is 100 times higher than that of silicon, high charge carrier mobility up to 2×10^5 cm^2 V^{-1} s^{-1} and exhibit ballistic charge transport which makes graphene have high electrical conductivity[45-47]. Graphene is also the strongest material, with regards to its elastic properties and intrinsic breaking strength[48]. Furthermore, exfoliated graphite flakes have been found to have extraordinary Young modulus values (>0.5–1.0 TPa)[49]. Graphene has high specific area (2630 m^2 g^{-1})[50] and thermal conductivity of 5.1 x 10^3 Wm^{-1} K^{-1} which is ten times higher than that of copper[51]. Other unique features of graphene include the ability to transmit light, resistance to chemicals, antibacterial potential, impermeability to gas, thermal stability and environmental friendly[52]. Individual graphene sheets are 0.34 nm thick and have an aspect ratio of 10^4 and higher. All the mentioned properties have led graphene to be an outstanding individual material as well as a better reinforcing material in the composites and also refer to as miracle material.

1.1.1.1 Mechanical Properties

The exceptional mechanical properties are influenced by the stable sp^2 bonds which forms the hexagonal lattice and resist the in-plane deformations. The mechanical properties of free-standing monolayer graphene were estimated using atomic force microscope (AFM) (Figure 2)[53].

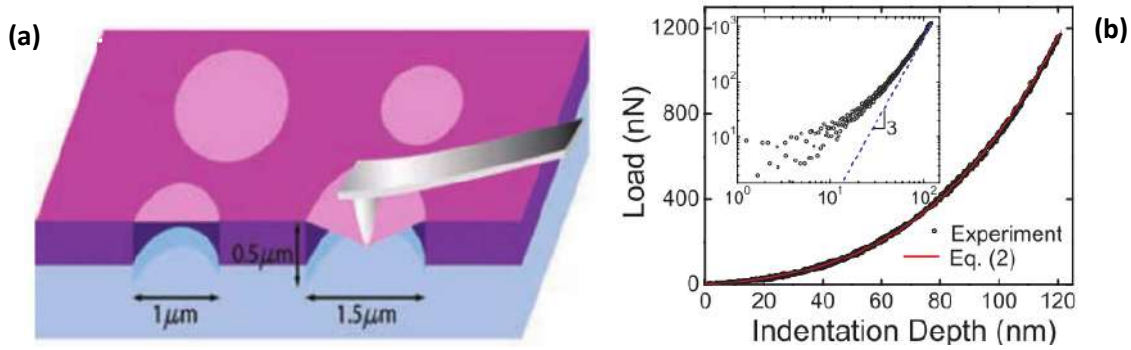

Figure 2 (a) Representation of nanoindentation setup on graphene (b) Loading-unloading curve with incrementing indentation depth[53]. (Figure adapted with permission from ref 53, Copyright 2008, The American Association for the Advancement of Science.)

Under uniaxial tension the isotropic elastic reaction is represented as

$\sigma = E\varepsilon + D\varepsilon^2$ – (1)

where

σ - symmetric second order Piola-Kirchhoff stress

E - Young's modulus

ε - uniaxial Lagrangian strain

D - third-order elastic modulus.

The maximum stress is represented as $\sigma_m^{2D} = \left(\frac{FE^{2D}}{4\pi R}\right)^{1/2}$

where

E^{2D} - second order elastic stiffness

R - radius of tip

F – Applied load.

The intrinsic strength and the second order stiffness value of graphene sheet without defect is estimated as 42 Nm^{-1} and E^{2D} = 340 ± 50 Nm^{-1} respectively. These values result in Young's modulus and third-order elastic stiffness of 1.0 TPa and -2.0 TPa respectively, for a defect free graphene sheet with a thickness of 0.335 nm[54]. Frank et al. deliberated the mechanical properties of suspended multilayer graphene sheets (thickness between 2 and 8 nm) by nanoindentation using AFM and extracted Young's modulus of 0.5 TPa[55]. Lee et. al. predicted the specific penetration energy in multilayer graphene under extreme dynamic supersonic impact and regarded graphene as the strongest material (~8-12 times stronger than sheets of macroscopic steel)[56]. Graphene exhibits specific penetration energy of 0.82 and 0.86 MJ kg^{-1} at the projectile velocities of 600 and 900 ms^{-1} respectively, which substantially overpasses steel at the same velocities (0.08 and 0.11 MJ kg^{-1}). Graphene delocalises the concentrated stresses during impact, thereby mitigating the premature failure.

Defects and wrinkling are inevitable during the synthesis and transmission of graphene on a specific substrate. These factors significantly alter the mechanical properties of graphene amongst all other properties. Using molecular dynamic simulations shear test was performed on zigzag graphene. The simulations reveal the fracture stress of planar morphology is 97.5 GPa, while that of wrinkled morphology is 60 GPa. The reduced fracture

stress is attributed to the softening of material[57]. Thus the choice of graphene plays a significant role in the reinforcing mechanism.

1.1.1.2 Thermal Properties

The thermal conductivity in single layer graphene (SLG) was determined using confocal micro-Raman spectroscopy by the non-contact method[58]. The thermal conductivity estimated using Raman spectroscopy works well in graphene, since the one atom thick layer allows the speedy heat transfer (in-plane). Unlike, in bulk crystalline material where the heat escape is three dimensional. Schematic representation of the experimental setup and the corresponding Raman spectrum of SLG is shown in Figure 3.

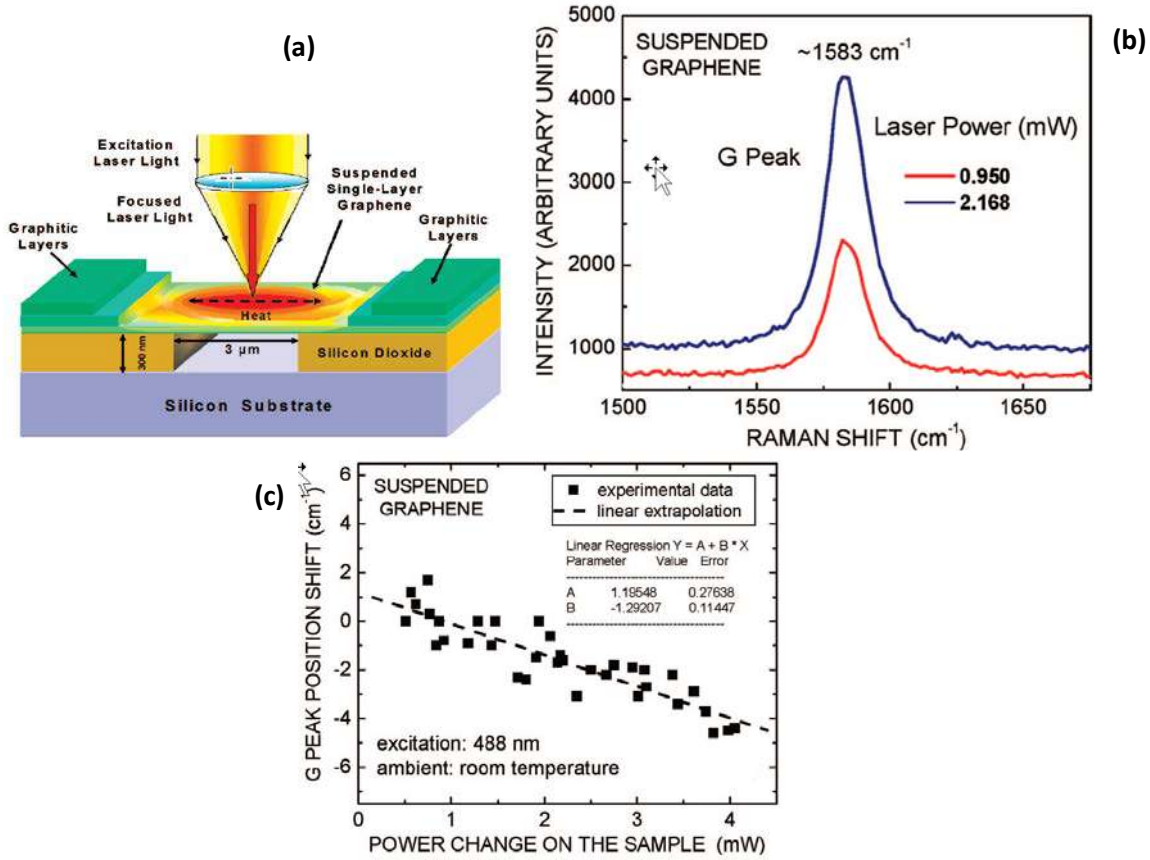

Figure 3 (a) Representation of laser focused on graphene layer during the experiment (b) Raman spectrum with G peak region logged at different laser excitation power (c) G peak spectral position shift vs change in total dissipation power[58]. (Figure adapted with permission from ref 58, Copyright 2008, American Chemical Society.)

Thermal conductivity is expressed as

$$K = \left({}^{1}/_{2}\,\pi h\right)\left(\frac{\Delta P}{\Delta T}\right) \text{ - (2)}$$

Where

h - thickness of SLG

ΔT - intrinsic temperature rise owing to variation in heating power ΔP. The final expression of thermal conductivity is given as

$$K = \chi G \left(\frac{L}{2hW}\right)\left(\frac{\delta\omega}{\delta P}\right) - (3)$$

$\delta\omega$ is the small change in peak position due to change in δP and is calculated from slope of the curve in Figure 3(c). The temperature coefficient for graphene χG is -1.6 x 10^{-2} cm^{-1}/K[58]. Thus the averaged thermal conductivity of SLG is ~4.8 x 10^3 to ~5.3 x 10^3 W/mK. The calculated thermal conductivity of SLG is close to or higher than high end values of single-walled/multi-walled carbon nanotubes (CNT) (shown in Table 1)[59].

Table 1. Thermal conductivity of graphene and other carbon materials estimated at room temperature [59, 60, 61, 62]

Sample Type	*K* (W/mK)	Method	Comments
SLG	~4840-5300	Optical	Suspended individual sheet
Few layer graphene (2 to 4 layers)	~2800-1300	Laser	Suspended individual sheet
Graphene ribbons ~65 nm wide	~ 100	Electrical	Suspended individual sheet Decreased thermal conductivity is due to edge disorder and dimension of graphene.
Pillared graphene structures along graphene direction ~3.6 – 9.1 nm^2	~33 – 86	Simulation	Thermal conductivity typically depends of the graphite sheet size and the inter pillar distance
Multi-walled-CNTs	> 3000	Electrical	Suspended individual sheet
Single-walled-CNTs	~ 3500	Electrical	Suspended individual sheet
Single-walled-CNTs	~ 1750-5800	Optical	Aggregates or bundles

In an ideal graphene structure, the carbon atoms are covalently bonded in a layer. When these atoms in graphene interact with the heat source, they start to vibrate and the vibrations are transferred to individual atoms due to the strong interactions of the covalent bond. In other words, the heat transfer in graphene is similar to the conduction in crystalline materials. Further, it is witnessed that heat is transmitted as phonon waves exhibiting a ballistic diffusive regime[63]. In multilayer graphene nanoplatelets, due to weak van der Waals forces between the layers, the vibrations in one layer are not transmitted to subsequent layers, hence anisotropic heat conduction exists[58]. The other forms of graphene exhibit lower thermal conductivity compared to single and multi-layer graphene due to the edge defects and dimensions of graphene[61,62]. Recently, graphene based nanofillers have emerged as a promising filler in polymers demonstrating higher thermal conductivity enhancements compared to CNTs[64-67].

1.1.1.3 Electrical Properties

Holes and electrons act as charge carriers in the graphene material resulting in high electrical conductivity. Six electrons of a carbon atom are configured as two in the inner and four in the outer shell. The outer electrons are involved in bonding. However, in the 2D plane of graphene each atom is bonded to three other atoms leaving behind a single electron in the third dimension which is in charge for electrical properties. These highly-mobile electrons are known as pi (π) electrons and are situated on the either sides of graphene sheet. The electronic properties of graphene are due to the bonding and anti-bonding of the pi orbitals[68].

It has been reported that electron mobility in graphene is high, and the electrical conductivity of graphene is close to 6000 S cm^{-1}[69]. Thus when graphene is used as a shielding material, the high conductivity leads to thin skin depth, resulting in the deterioration of the electromagnetic field. Typically, reflection loss at interfaces between any two materials is dependent on the difference between the characteristic impedance of the shield and the nearby material. Hence, electrical conductive material such as graphene is useful for electromagnetic interference (EMI) shielding[70].

1.1.2. Macroscopic architectures of Graphene

Benefiting from various syntheses strategy, graphene has materialized as a nanomaterial that can be developed into architectures of macroscopic scale. The multiple interactions in graphene such as π-π interactions, van der Waals forces, electrostatic forces, and dipole-dipole interactions are responsible for the development of various architectures such as films, gels, fibers and porous network[71]. Graphene fibers can be spun from aqueous graphene oxide liquid crystals followed by reduction. The chemically reduced graphene fibers are strong, flexible and highly conductive. These reduced fibers exhibit electrical conductivity up to ~2.5x10^4 Sm^{-1}, fracture strength of 140 MPa and Young's modulus of 7.7 GPa, despite maintaining significant fracture elongation of ~5.8%[72]. Thermal annealing of intercalated small sized and large sized graphene oxide aligned graphene fibers achieved an enhanced thermal conductivity (1290 Wm^{-1} K^{-1}), electrical conductivity (2.21x10^5 Sm^{-1}) and tensile strength (1080 MPa)[73]. Two-dimensional graphene paper/film is fabricated by vacuum filtration method[74] and solution deposition methods[75,76]. For instance, thickness controlled large area free-standing graphene paper was synthesised by electro-spray deposition with an uninterrupted roll-to-roll process. The thermally annealed (2200 ^{o}C) films resulted in exceptional thermal and electrical conductivity[77]. Three-dimensional foam-like graphene networks are

fabricated by template-directed CVD[78], ice-segregation induced self-assembly[79], hydrothermal[80], chemical reduction[81] and electrochemical[82] methods. Although these techniques allow effective dispersion of graphene sheets three-dimensionally, the foamed structure is irreversibly damaged under mechanical deformations due to the brittleness. However, polymer supported graphene foams display good mechanical[83] and electrical properties[79] and are structurally stable.

The atomically thin material graphene, possessing unique mechanical, thermal and electrical properties can provide protection in harsh operating conditions when reinforced in composites. In addition, synthesis of graphene sheets into macroscopic architectures is one of the unique capability compared to other nanoparticles and carbon-based materials which favor in tailored morphologies of graphene-reinforced composites.

2. Properties of graphene-polymer nanocomposites

The primary aim of reinforcing graphene into polymers is to improve the properties of composites for potential applications in several industries. Many reviews have been published to discuss the enhancement of composite properties due to graphene reinforcements. However, the performance of graphene based polymer composites in harsh operational conditions has not been yet reviewed comprehensively. Hence, the present review summaries some of the prospective applications of graphene-polymer composites which are suitable in harsh environments to gain a better purview of the material in focus.

2.1 Investigation of mechanical properties at cryogenic temperature (CT)

As previously discussed the exceptional properties make graphene an ideal choice for reinforcement. While most of the mechanical properties of graphene based polymer composites are evaluated under ambient temperature, it is equally important to diagnose the potential of these composites when they operate at cryogenic temperatures. Shen et al. studied the reinforcing potential of graphene in epoxy composites at cryogenic temperature. The composite tensile strength increases with the increase in graphene concentration and reaches the maximum at 0.1 wt.% concentration. Percentage increase in tensile strength witnessed at room temperature (RT) and 77 K (CT) is 3.5% and 17.1% respectively[84]. Compared to the reinforcing effect of MWCNTs in Epoxy composite at CT, less concentration of graphene was sufficient to enhance the cryogenic mechanical performance (Figure 4)[85,86].

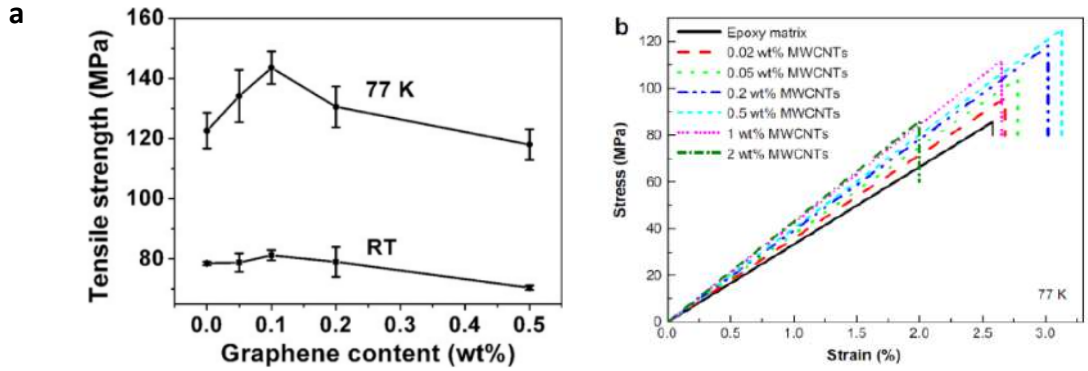

Figure 4 (a) Effect of graphene content in composite on the tensile strength at different temperature. (Figure adapted with permission from ref 84, Copyright 2012, Elsevier.) (b) Stress-Strain curve of MWCNTs/Epoxy at CT. (Figure adapted with permission from ref 85, Copyright 2009, Elsevier.)

Significant improvement in properties is witnessed when the polymer matrices is reinforced with chemically functionalized graphene. Hussein et al. reported a good strengthening and toughening behavior of graphene oxide (GO)- poly(p-phenylene diamine) (PDA) nanoparticles in epoxy without much effect on the modulus at RT and CT. The approach involved preparation of GO-PDA hybrid, followed by incorporation in epoxy and curing. RT evaluation of tensile strength, Young's modulus and fracture strain showed an increase upto 68.6 MPa, 1.52 GPa and about 11.14% respectively, with 0.05 wt% of nanoparticles. However, the mechanical properties of composite displayed a significant improvement at CT. The modulus at CT is twice the value at RT which is due to the restricted mobility of the polymer chains at CT. But, the strength and fracture strain exhibit a different trend at CT, where higher concentration is effective in improving these properties. The reinforcement is strong at CT due to the mismatch in CTE (between the matrix and nanoparticles) and the functionalization enhances the interfacial strength and matrix-filler interlocking. Therefore, during fracture de-bonding of GO-PDA, voids are formed. Figure 5a and b show the SEM micrographs of the fractured surface and 5c and d show the mechanism of fracture at CT and RT. In functionalised graphene nanocomposites, during the toughening mechanism the matrix

experiences shear yielding phenomenon at CT, rather than interface de-bonding and crack deflection which is predominant at RT[87].

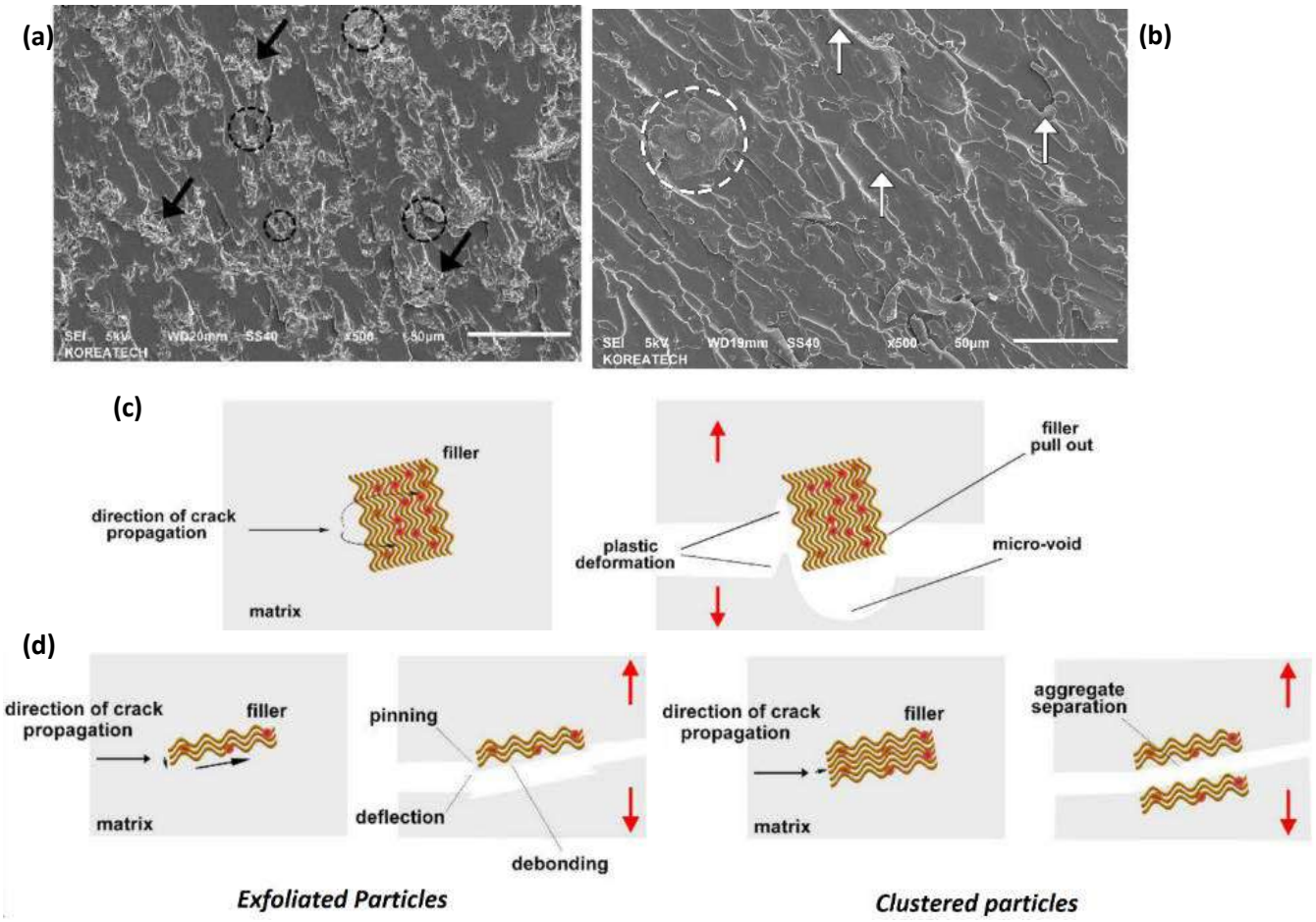

Figure 5: SEM micrographs of fractured surface at (a) CT -120 °C (b) RT 25 °C. Schematic of fracture mechanism (c) at CT and (d) at RT. (Figure adapted with permission from ref 87, Copyright 2017, Elsevier.)

In another study, polydopamine (PA) and polyetheramine (T403) grafted polydopamine (T403-PA) functionalized GNPs (0.1wt%) were reinforced in the epoxy matrix. The cryogenic tensile strength of PA/GNP/Epoxy and T403-PA/GNP/Epoxy composites increased by 26.3% and 34.5% respectively. In addition, the cryogenic impact strength of the of PA/GNP/Epoxy and T403-PA/GNP/Epoxy composites also increased by 50.1% and 64.5% respectively[88]. Thus functionalization has resulted in significant interfacial interactions between the filler and matrix, which ensured improved cryogenic mechanical properties.

Several recent improvements include the fabrication of multi-component graphene polymer nanocomposites with carbon fibers, glass fibers, silica nanoparticles or silane functionalized nanoparticles for improved cryogenic mechanical properties[89-93]. Li et al. revealed an effective approach to improve the cryo-mechanical properties of short carbon fibers/polyethersulfone (SCF/PES) composite. A major enhancement in cryogenic mechanical properties of composites was witnessed using GO coated SCF surface. A comparison of the enhancement of tensile and flexural strength at CT and RT for PES nanocomposite is shown in Figure 6. According to SEM micrographs (Figure 7) of failure surfaces, the space between the pulled-out fiber and the matrix reduces and eventually disappears at CT. Further, the extent of matrix attached to the pulled-out fiber coated with GO is significant at CT compared to RT, which is the reason for superior cryogenic mechanical properties[91].

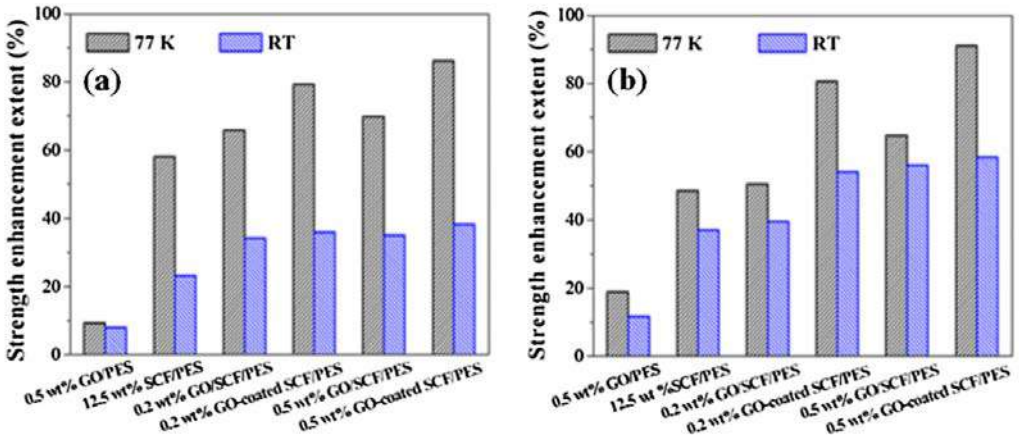

Figure 6 Comparison of property enhancement at CT and RT: (a) tensile and (b) flexural strength. (Figure adapted with permission from ref 91, Copyright 2016, Elsevier.)

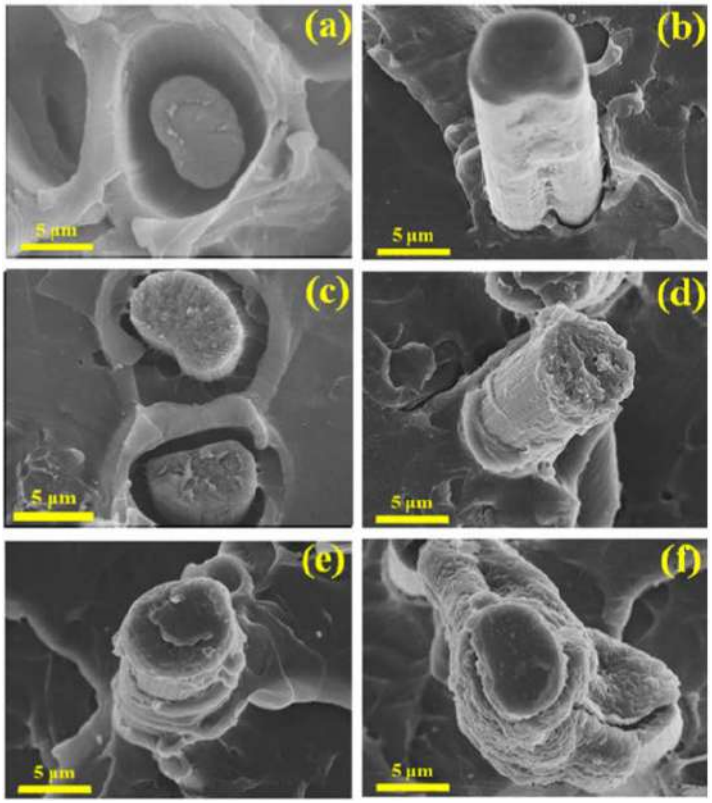

Figure 7 SEM micrographs of the failure surfaces of SCF/PES composite (a) at RT and (b) at 77 K, GO (0.5 wt%) and SCFs (12.5%)in discrete quantities in composite (c) at RT and (d) at 77 K and 0.5 wt% GO-coated composite (e) at RT, and (f) at 77 K. (Figure adapted with permission from ref 91, Copyright 2016, Elsevier.)

Ghosh et al., has predicted the flexural properties of multilayer graphene (MLG) embedded glass fiber/epoxy (GE) composites at different temperatures (-196, 30, 70 and 110 °C) (Figure 8)[92]. The mechanical property of MLG composites is greatly enhanced at CT compared to the RT or elevated temperature. The flexural strength, and modulus of 0.1 wt% composite increased by 23.7% and 20.7% respectively over neat GE.

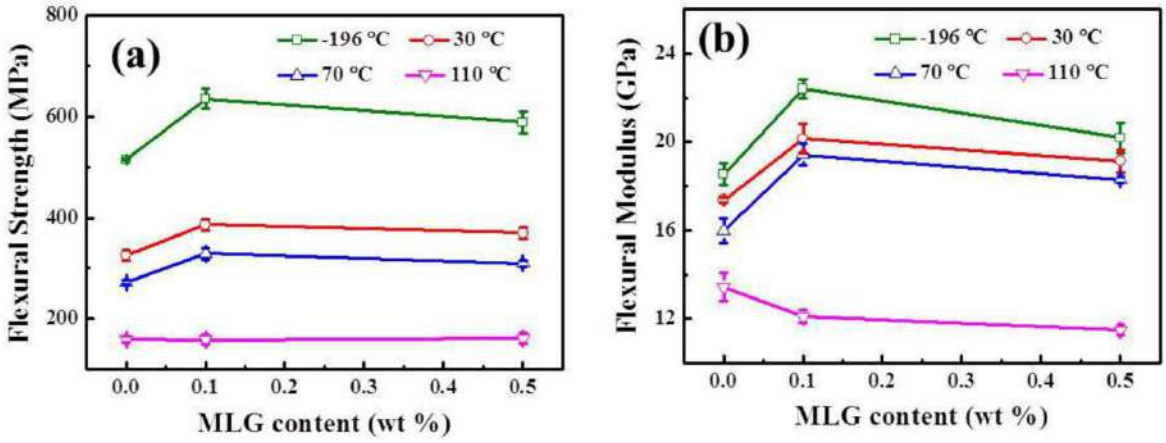

Figure 8 Flexural characteristics of MLG / GE composites at various MLG concentration and temperature (a) Strength and (b) Modulus (Figure adapted with permission from ref 92, Copyright 2018, Elsevier.)

In another study, Jiang et al. measured the cryo-mechanical properties of 3-aminopropyltriethoxysilane (APTES) surface modified silica nanoparticles functionalized GO (SATPGO)/epoxy nanocomposites. Interestingly the tensile strength and modulus showed a significant improvement at CT than at RT (Figure 9a and b). However, the impact strength at CT is lower than at RT for neat epoxy and composites (Figure 9c), which is due to the reduced molecular movement of the matrix. Therefore, during the impact test there is a brittle failure of the composite at CT[93].

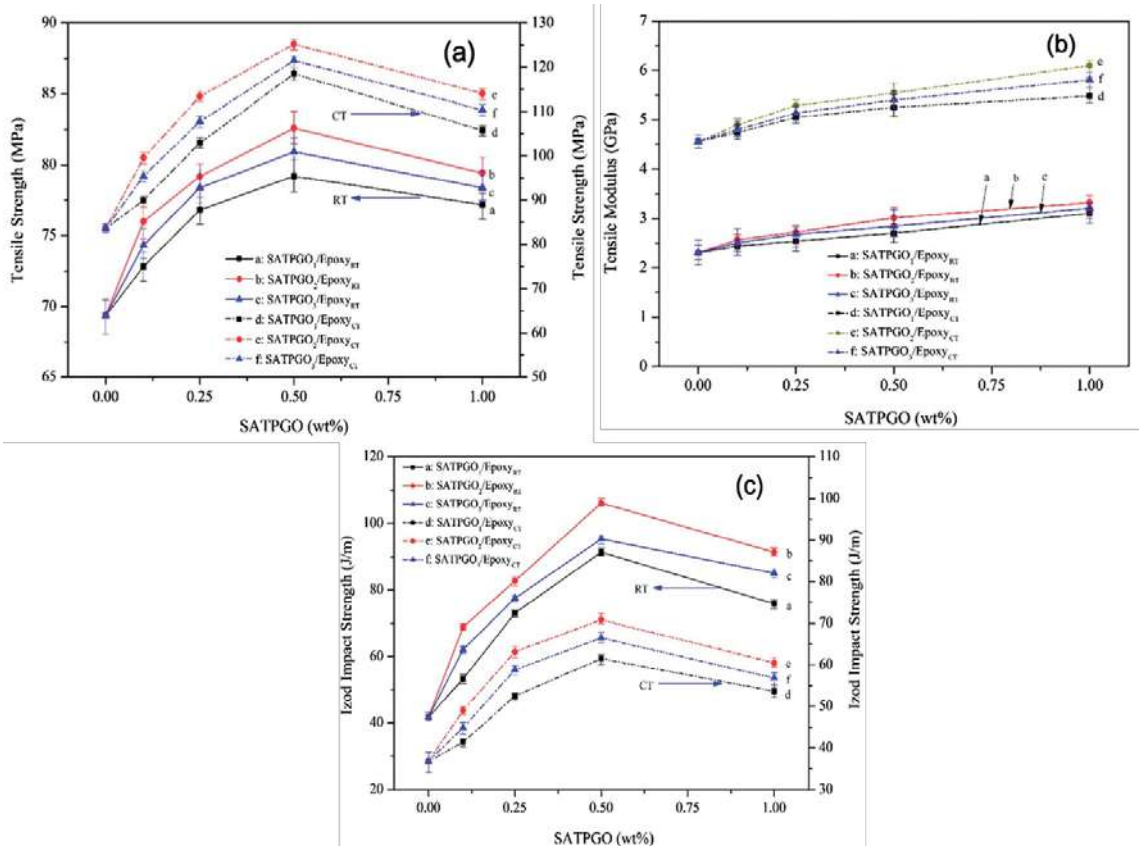

Figure 9: Mechanical properties of functionalised GO - epoxy composites at RT and CT. (a) Tensile strength, (b) tensile modulus and (c) Izod impact strength (Figure adapted with permission from ref 93, Copyright 2014, Royal Society of Chemistry.)

Impact strength is increased by 154% at room temperature and 92% at CT (Figure 9c). A similar trend in impact behavior was observed in GO reinforced epoxy composites at RT and CT[84] and polydopamine functionalized GNP-epoxy nanocomposites[86].

It is evident that graphene or multicomponent graphene reinforced composites possess outstanding mechanical properties at CT than at RT. The clamping stress caused at CT on graphene-polymer interface owing to the mismatch in CTE is recognized as the strengthening mechanism. Thus, by tailoring the graphene reinforcements in terms of concentration and functionalization can result in composites with enhanced mechanical properties suitable for cryogenic conditions. These composites are suitable for applications such as hydrogen storage tanks in fuel cell electric vehicles, autoclave tanks for space applications and structural components in aerospace industries where composites are subjected to low temperature environment.

2.2 Investigation of ballistic impact behavior

Hypervelocity impact (HVI) causes shock waves which induces enormous energy on both the impact and the target materials. The extreme shock pressures induced on the targeted materials, leads to stresses which are much higher than their strength. This is one of the vital phenomenon to be considered during the design of high-performance space structures[94]. The accelerating motion of the projectiles in outer space causes ballistic deformation (> 10^5 /sec.) on the space structures. To prevent aerospace vehicles from such damages, the design of structures for space should consider the outcome of impact loading on various components at different velocities. Based on the velocity, impact loadings were categorized as low (3.9 km/s), high (5.2 km/s) and hyper velocity (6.9 km/s) impacts.

Lee et. al. performed a miniature ballistic test on multilayer graphene (MLG – 10 to 100 nm which corresponds to 30 to 300 layers of graphene) using laser-induced projectile impact test (LIPIT) at firing speed of <3km/s[56]. Penetration experiments show MLG experiences tensile stretching leading to a cone shape followed by the onset of radial cracks which nearly trace the crystallographic directions and spread outward beyond the impact area (as shown in Figure 10). The cone deformation in MLG experiences a radial speed of 1950 and 2560 m/s at 500 and 900 m/s, which is very close to the wave speed predicted by analytical methods.

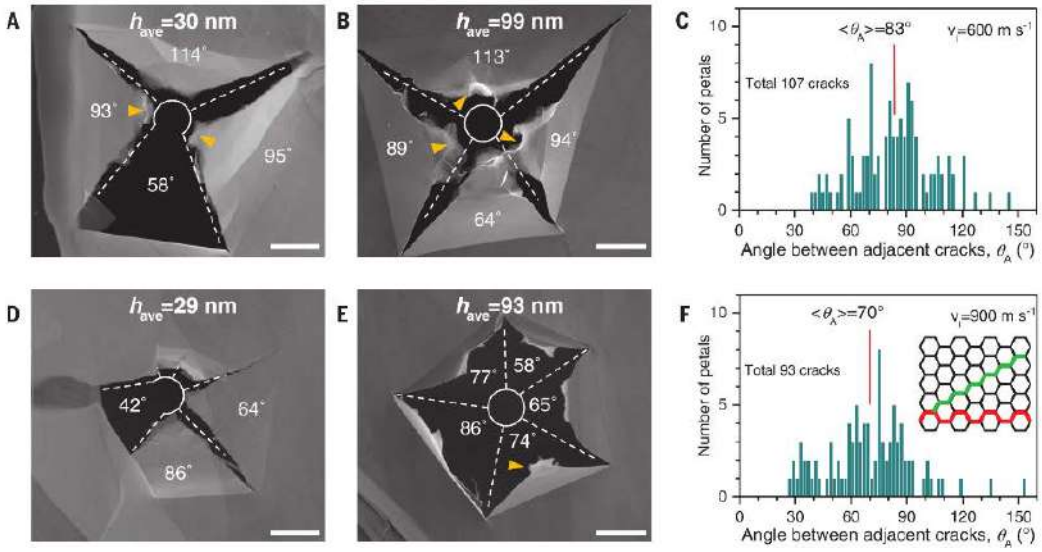

Figure 10 Deformations in MLG membranes due to penetration experiment. (A, B, D and E) SEM micrographs of damaged MLG showing radial cracks, petals, folds and snap-back. Distribution of angle between adjacent cracks (C)at v_i=600ms^{-1} and (F) at v_i=900ms^{-1} with inset showing armchair (red) and zigzag (green) directions. The strike face area is represented as circle in the SEM. Scale bars: 5 µmm. (Figure adapted with permission from ref 56, Copyright 2014, The American Association for the Advancement of Science.)

The specific penetration energy of MLG (as shown in Figure 11) is estimated to be higher than that of steel, due to the delocalization behavior. However, during multiple hits the delocalization effect could result in broader penetration holes and eventually fails the ballistic potential of MLG. The potential weakness in MLG can be overcome by composite formation thereby deflecting the crack propagation. Thus, MLG can afford outstanding impact energy delocalization during supersonic penetrations, which inspires the opportunities for fabrication of bulletproof vests.

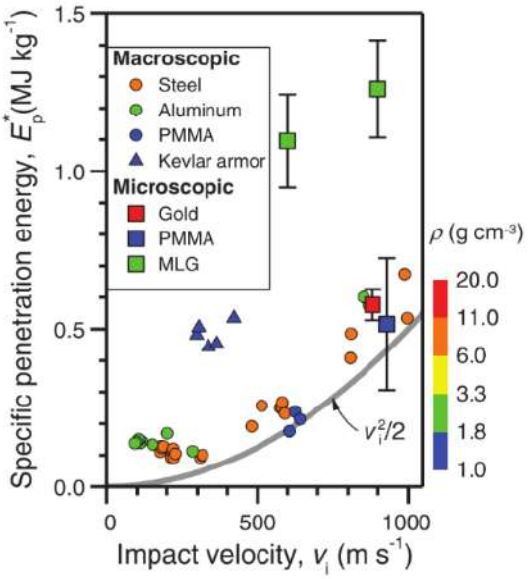

Figure 11 Specific penetration energy of microscopic and macroscopic materials at various impact velocities. (Figure adapted with permission from ref 56, Copyright 2014, The American Association for the Advancement of Science.)

Masta et. al. investigated the quasi-static and projectile impact loading behaviour of multilayer graphene (MLG - 10 μm) / polyvinyl alcohol (PVA) composite film [95]. The ballistic limit of the composite films with ~35 vol.% MLG is greater than the Al films. However, the ballistic resistance of pristine PVA film is superior to Al and PVA/MLG films due to the higher ductility. (Figure 12).

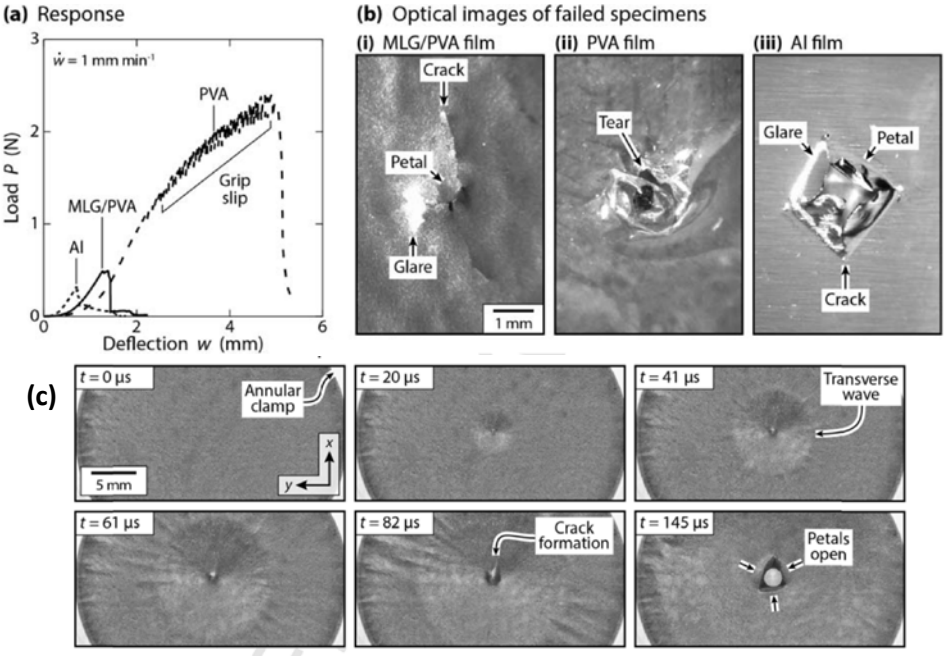

Figure 12 (a) Load-displacement response under QS transverse loading (b) Optical images of failed specimens (c) Rear view of the composite film at different time impacted by 20 mg projectile at 16.7 m s^{-1}. (Figure adapted with permission from ref 95, Copyright 2017, Elsevier)

Besides hypervelocity impacts, traditional impact tests were conducted on graphene reinforced composites to investigate their impact behavior. Kusar et al. studied the impact behavior of GO reinforced epoxy nanocomposites[96]. Considerable enhancement in impact strength of 45.4% was achieved with 1 wt% GO. However, functionalized GO exhibited significant improvements in impact behavior of composites. Qi et al. fabricated epoxy composites with thermotropic liquid crystalline epoxy grafted GO (TLCP-GO) as reinforcing filler. Impact strength increased by nearly 96% for 1 wt% TLCP-GO loading[97]. Whereas, in Nylon 12 by

reinforcing with 0.6wt% of functionalized GO a significant improvement of 175% in impact failure energy is witnessed[98].

Graphene also exhibited a synergistic effect in impact strength in hybrid nanocomposites. 5wt% of exfoliated GNP coated glass fiber (GF)/ epoxy composites showed 8% growth in impact strength compared to the pristine composite[99]. Similarly, 0.1 wt% GNPs in basalt fiber/epoxy composite exhibited 16% improvement in impact strength. Multiple fiber breakages, fiber pullouts and delamination are the major damage mechanism withnessed due to GNP incorporation in composites[100]. Avila et al. performed a ballistic test on fiberglass/epoxy/GNP hybrid nanocomposites (Figure 13). Hybrid composite of 3wt% graphene in pure glass fiber/epoxy was fabricated and impacted by 9 mm projectile with the speed of 380 m/s as per NIJ standard. An interesting observation was that a 9mm projectile was entrapped in the hybrid composite and the copper shell in the projectile has suffered deformation inside the composite. An increase in the coefficient of friction caused by the GNPs is responsible for such deformations[101].

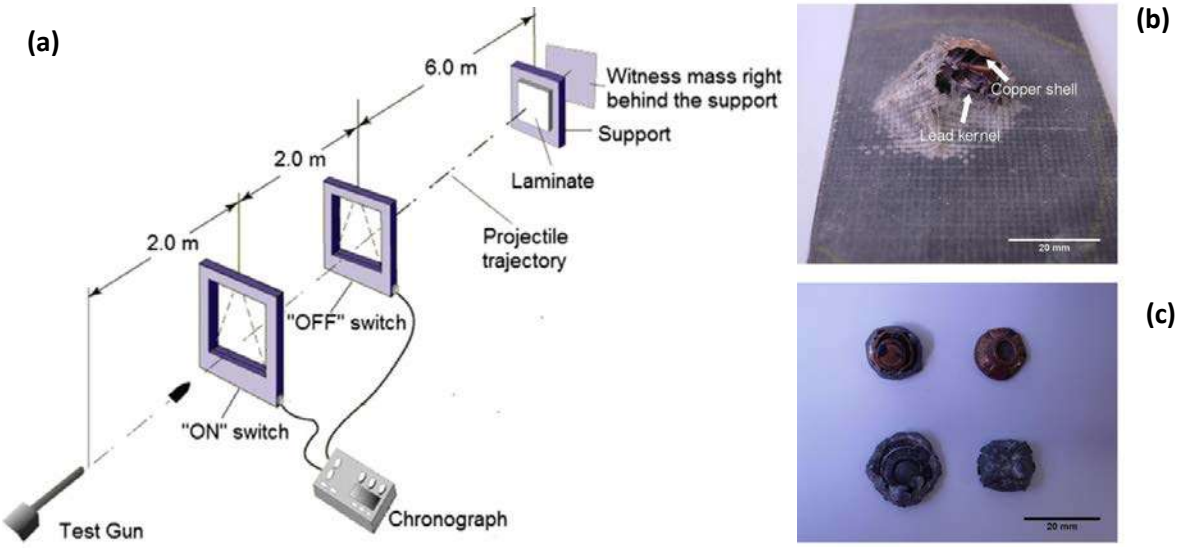

Figure 13. (a) Test apparatus representation. (b)Digital photograph of 9mm projectile trapped on 3 wt% graphene (c) Deformed projectiles. (Figure adapted with permission from ref 101, Copyright 2011, Elsevier)

Thus the incorporation of GNPs strengthened the interface between the matrix and fiber and provided more energy absorption capability and good load transfering ability between the fiber and matrix. Although the above studies indicate graphene as a potential reinforcement to sustain ballistic impact, a comprehensive study is still required to understand the behavior of composites. Such ballistic impact sustainable graphene based composites finds potential application in lightweight automotive structures, body armours and other wearable devices.

2.3 Investigation of thermal properties

Thermal management is the vital feature for safety, reliability, and performance of several applications such as electronic assembly and packaging, solar energy devices, medical devices, automobile, aerospace structures etc.[102]. These advanced applications coupled with emerging technologies such as flexible/transparent electronics, demand flexible and lightweight thermal management materials. Traditional heat sink materials such as ceramics and metals are heavy and bear low flexibility causing a severe bottleneck to the developing technologies[103].

Recently, graphene based polymer composites have drawn wide interest owing to their superior thermal conductivity. GNPs have resulted in significant enhancement of thermal conductivity in epoxy composites[104]. Maximum thermal conductivity enhancement (TCE) of 1422% was achieved by ball milling technique for the filler loading of 25 wt%. It is also evidenced that the composite preparation technique impacts the thermal conductivity of the composite. For instance, sonication method yielded only 900% enhancement at the same filler concentration (Figure 14). In addition, the thermal conductivity also exhibited dependence on the milling time. Thus the thermal conductivity enhancement is attributed to (i) homogenous dispersion of GNP in composite, (ii) the better quality and high exfoliation degree of GNP and (iii) better interfacial-interaction between matrix and filler.

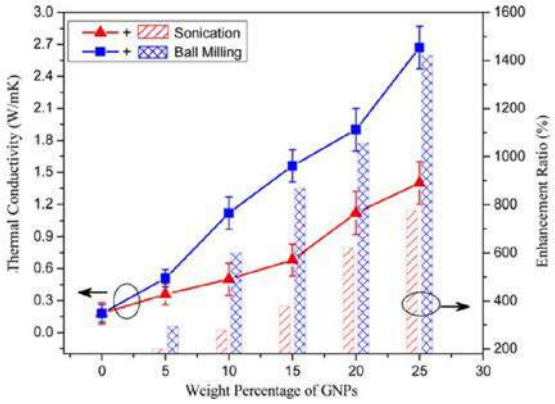

Figure 14 Thermal conductivity of epoxy/GNP composites fabricated via. different methods as a function of GNP weight percentage. (Figure adapted with permission from ref 104, Copyright 2014, John Wiley and Sons)

Similarly, applying compressive forces during the dispersion of GNP in epoxy has a significant outcome on the thermal conductivity[105]. The effect of GNP lateral dimension and defect density on TCE is reported. The high compressive forces exhibited by zirconia balls during the planetary centrifugal mixing technique resulted in GNP with large lateral dimensions and small defect density. The homogenously dispersed GNPs with greater GNP transport pathways exhibited high isotropic TCE of 6800% for 1 vol% GNP loading.

Hybrid graphene composite has resulted in improved thermal transport properties. For instance, Shahil et al. synthesized graphene-MLG hybrid epoxy nanocomposites with high TCE factor at a low level of filler loading. The laser flash measurements show high enhancement of thermal conductivity up to 2300%, for a filler loading of f=10% (as shown in Figure 15a). The unusual enhancement is due to the (i) high intrinsic thermal conductivity, (ii) geometrical shape, (iii) high flexibility of graphene and MLG, (iv) low Kapitza resistance at the interface and (v) optimum concentration of fillers with different lateral size and thickness[106]. TCE shows a dependency on filler loading without any thermal percolation threshold. Further, the dependence of thermal conductivity on the temperature at different graphene concentration demonstrates Umklapp phonon scattering characteristics as in crystalline materials (Figure 15b). Thus the heat is transferred through the crystalline phases of graphene – MLG and it is absent in amorphous solids such as epoxy.

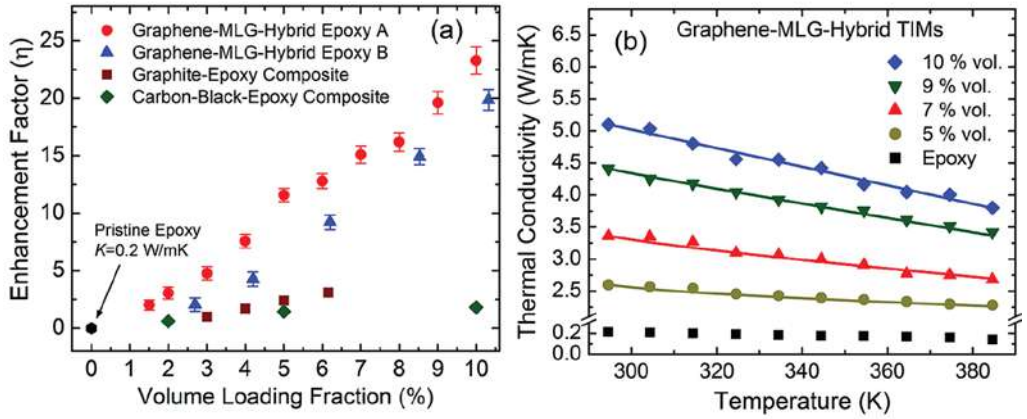

Figure 15 TCE in the graphene-MLG/epoxy nanocomposite (a) TCE of different composites at different loading fractions (b) Dependence of TC on temperature for different loading. (Figure adapted with permission from ref 106)

In addition to composite preparation technique and hybridization of composites, alignment of graphene in composite plays an important role in thermal transport. The thermal conductivity of 33.5 W/mK was witnessed in the aligned MLG/epoxy composite (AG/E) containing 11.8 wt% filler content. The aligned structure in composite results in increasing thermal coductivity with temperature varying from 40 °C to 90 °C (Figure 16). The AG/E composite posses a TCE value of ~16670% which is higher than any other reported epoxy composites[107]. Thermal conductivity also shows dependence on the aligning angle of graphene and possesses good thermal stability over three heating and cooling cycles.

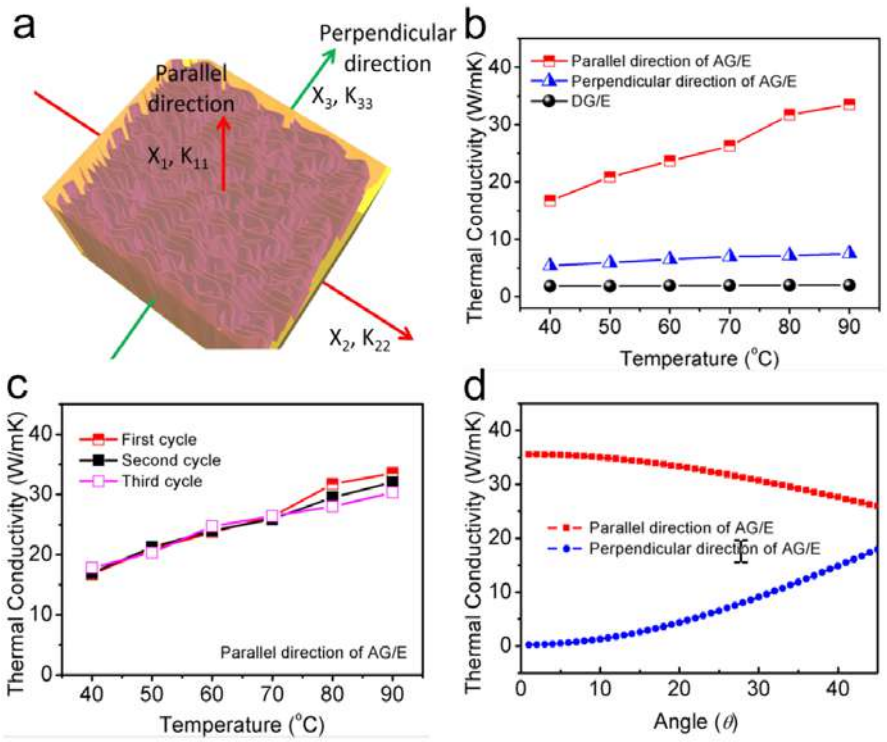

Figure 16 (a) Representation of the parallel and perpendicular direction of TC in aligned composites (b) TC vs temperature in aligned and dispersed composites (c) TC vs temperature in aligned composite at different heating cycles (d) Theoretical TC vs alignment angle. (Figure adapted with permission from ref 107)

Zhang et al. fabricated horizontal and vertical aligned graphene epoxy composites as a heat sink for LED lamps[108]. The continuous graphene film acts as a channel for the heat removal process. Thermal conductivity as high as ~385 W/mK was achieved in vertically aligned composite compared to horizontally aligned composite which was 0.81 W/mK at the filler concentration of 44 vol%. The drastic enhancement of 3570% in the vertical direction is attributed to the bi-directional heat dissipation mechanism in the composites (Figure 17).

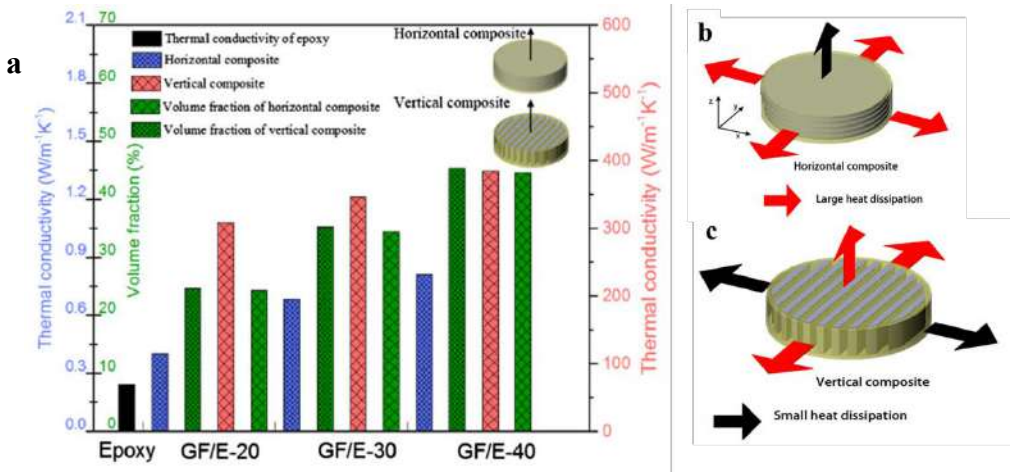

Figure 17 (a) Thermal conductivity of aligned composites. Mode of heat dissipation in the aligned composite. (b) Horizontal (c) Vertical. (Figure adapted with permission from ref 108, Copyright 2018, Elsevier)

It is observed that graphene with specific orientation (such as aligned or 3D structures) has a strong influence on thermal conductivity compared to the randomly oriented graphene (Table 2). The oriented structures of graphene in composites act as conductive channels thereby favoring efficient thermal conductivity. The heat transfer system in these composites is realized through their unique aligned morphology which finds potential application in microelectronics operating at high power requirements.

Table 2: Thermal conductivities of oriented graphene based composites

Filler	Matrix	Filler content	Thermal conductivity W/mK	Thermal conductivity enhancement (%)	Orientation of graphene	Ref
Multi layers of graphene	Epoxy	11.8 wt%	33.54	16670	Aligned structure	107
Graphene Films	Epoxy	44 vol%	884.9	3570	Vertically aligned	108
Graphene Films	PDMS	92.3 wt%	614.85	3329	Vertically aligned	109
Graphene	Epoxy	0.92 vol %	2.13	1231	Vertically aligned and interconnected	110
Graphene	PVDF	10 wt%	1.47	673	Cellular framework	111
Graphene	PP	10 wt%	1.53	595	Cellular framework	111
Graphene	PVA	10 wt%	1.43	580	Cellular framework	111
Graphene	PE	10 wt%	1.84	457	Cellular framework	111
Graphene	PA6	2.0 wt%	0.847	300	3D Foam	112
Graphite nanoflakes	PA6	12 wt%	2.49	678	Intercalated	113
Graphene nanoflakes	PVDF	25 vol %	10	50	Oriented	114
GO + GNP	PEG	0.45 wt% GO	1.43	361	Hybrid aerogel	115
		1.8 wt % GNP			GO- Network structure	
					GNP- uniformly dispersed	
rGO	TPU	1.04 wt%	0.8	345	Segregated	116
rGO	PVDF – hexafluoropropylene	27.2 wt%	19.5	9000	Self-aligned	117
rGO	Cellulose	1 wt%	12.6	1046	Layer-by-layer	118

Graphene in combination with micro/nano metal nanoparticles has also exhibited a synergistic effect on thermal conductivity. Graphene incorporated in commercially available silver-epoxy composites, exhibited a 500% increase in thermal conductivity in the temperature range from 300 to 400 K for 5 vol% graphene loading[119]. Im et al. optimized the weight fraction of GO (50 wt%) in MWCNT (0.36 wt%) epoxy wetted composites for a remarkable enhancement in thermal conductivity[120]. The voids in the composites are effectively occupied by GO, forming a thermal conducting path.

Thus, graphene based composites exhibit significant enhancement in thermal conductivity. However, the degree of enhancement is influenced by the choice of composite preparation technique and the alignment of graphene within the composites.

2.4 Investigation of de-icing behavior

In the present world, static equipment such as radio masts, instrumental housings or power lines and dynamic aero structures such as aircrafts, wind turbine blades and rotor blades are exposed to varying temperature conditions[121].

At low temperatures, development of ice layers on these structures can cause a potential functional loss, forfeiture of shape and structural integrity leading to catastrophic consequences. Existing measures to mitigate the ice establishment include the dispersion of chemicals, cold gas boot system, weeping wing system and electrical heating of surfaces[122,123]. However, these approaches increase the overall weight of the structures and cause degradation of the substructures owing to the chemical reaction or localized heating, in addition, incur periodic maintenance.

Recent studies have focused on the Joule heating efficacy of graphene nanomaterials to develop efficient deicing systems. During Joule heating mechanism, a thin layer of ice at the interface of ice and the heated surface is melted to produce a layer of water underneath the ice. This mechanism weakens the adhesion of ice and facilitates the ice removal via. gravity, centrifugal force, air/wind or inflated pneumatic wrap[124]. In addition, Joule heating can be actively controlled through receiving feedbacks from integrated sensors and in turn, switched on and off in a timely manner.

For example, Volman et al. prepared robust graphene nanoribbon (GNR) based conductive composite coatings which are radio frequency (RF)-transparent. These composite coatings have the potential to mitigate the size and cost of deicing coatings for RF equipment shields in aviation or marine applications. The deicing capability was evaluated at -20 ºC and the ice melted in few minutes as the current passes through the GNR film. The change in resistance exhibited by composite coating is close to -10%, for temperature ranging from 20 ºC to 100 ºC. This change is in resistance is significantly smaller than those for metals (+30% from 20 ºC to 100 ºC). Such smaller resistance of GNR is very helpful for deicing applications[125]. Janas et al. have presented an overview of production methods for CNT and graphene based thin films for electro-thermal applications, including the deicing applications[126].

In another study, Raji et al. evaluated the potential of GNR stacks in epoxy, which serves as a tunable conductive composite for deicing surfaces with high ice deposit as in the leading edge of rotor blades[127]. 5 wt% GNR/epoxy composite coating generated Joule heating effect to remove 14 g monolith of ice (~1 cm thick) from a static helicopter rotor blade surface operating at -20 ºC. Figure 18 shows the process of composite fabrication followed by Joule heating and deicing behavior of a helicopter rotor blade segment. Minor variation in the thickness of the composite film resulted in varying resistance, which in turn produces different heating temperatures. Higher the resistance of a segment in the film results in higher temperature compared to the surrounding. The heat generated by the composite segments at different voltage are shown in Figure 19.

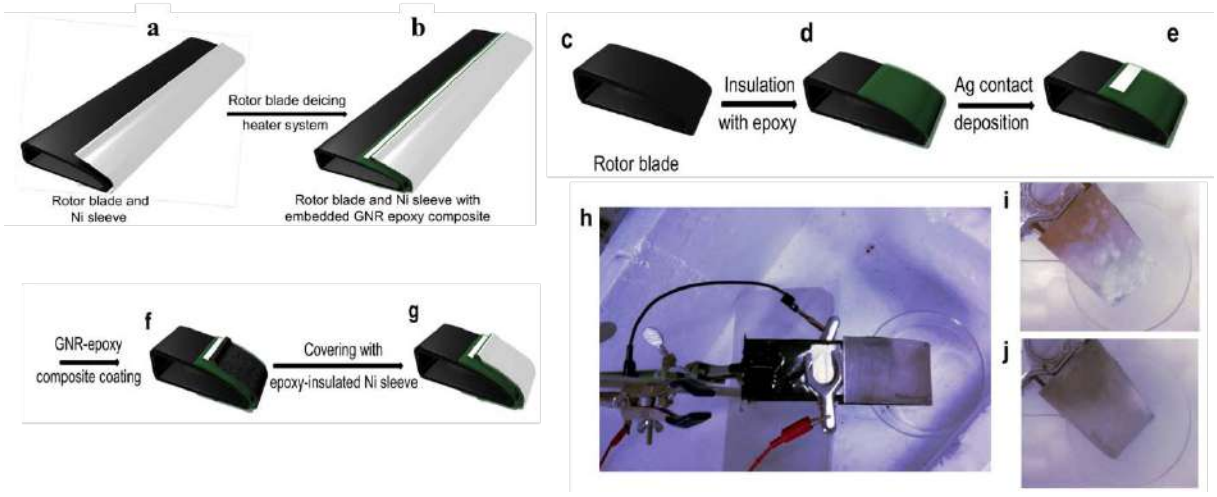

Figure 18 Helicopter rotor blade segment exhibiting Joule heating and deicing behaviour (a-b) Representation of the composite adhesive deposited on a rotor blade. (c-g) Steps by steps coating process on a rotor blade segment. (h-j) Image of deicing via Joule heating of a rotor blade. (h) The set-up before ice deposition. (i) After ice deposition and before applying a voltage. (j) After deicing. (Figure adapted with permission from ref 127)

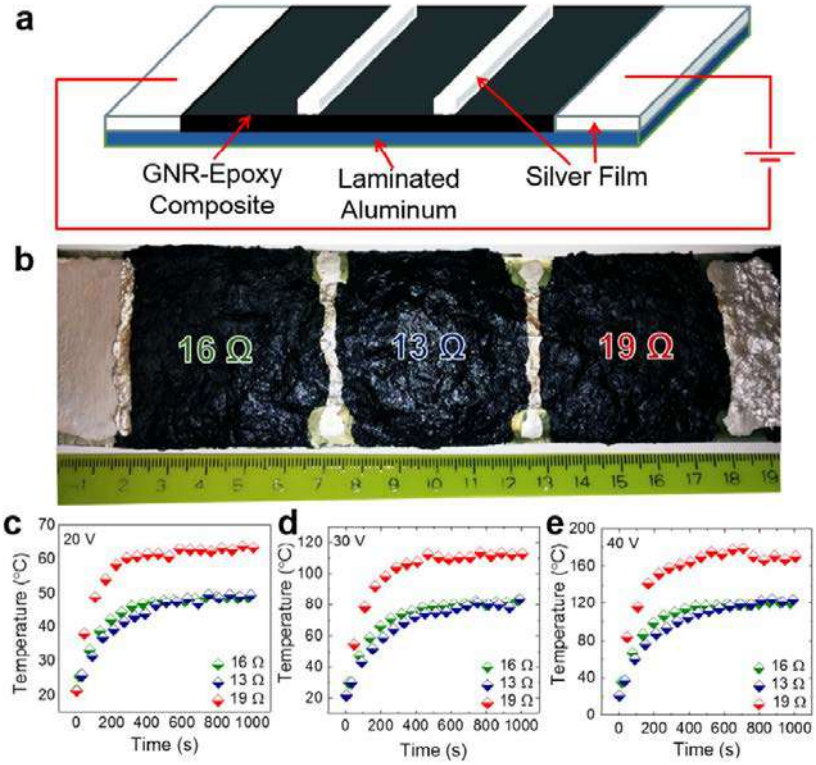

Figure 19 GNR-epoxy composite exhibiting Joule heating phenomenon. (a) Representation of a Joule-heated composite device. (b) Photograph of Joule-heated composite. The resistance across individual segments are displayed. Scale: cm. (c–e) Temperature generated by composite segments at different applied voltages. (Figure adapted with permission from ref 127).

Chen et al. validated the deicing phenomenon of graphene coating on composite surfaces by controlling the spraying process parameters. Graphene coating displayed a good heat transfer efficacy when the coating thickness is reduced and the applied pressure in the spraying process is high[128]. Further, Zhang et al, studied the Joule heating and anti-icing/ deicing behavior of robust and conductive graphene-paper/glass-fiber/epoxy (GP-GE) composites[129]. The composite exhibited consistent electro-thermal and structural stability for over 200 cycles with temperature varying from -20 to 90 °C. In order to envisage the joule heating performance, two cases were validated as in practical applications (1) pre-heating derived deicing characteristics and (2) direct deicing characteristics (Figure 20). The pre-heating strategy was utilized to demonstrate the anti-icing behavior by serving a low heating power of 300 W/m^2 up to the freezing point for 950 s (Figure 20a). The pre-heating strategy is a demonstration of cleaning composite surfaces in -15 °C harsh conditions within 1h using low heating power. On the other hand, a more rapid deicing phenomenon was witnessed in the composites with 10 mm thick ice slab formed within 2400 s. Large power input of 3000 W/m^2 deiced the composite surface within 365 s (Figure 20b).

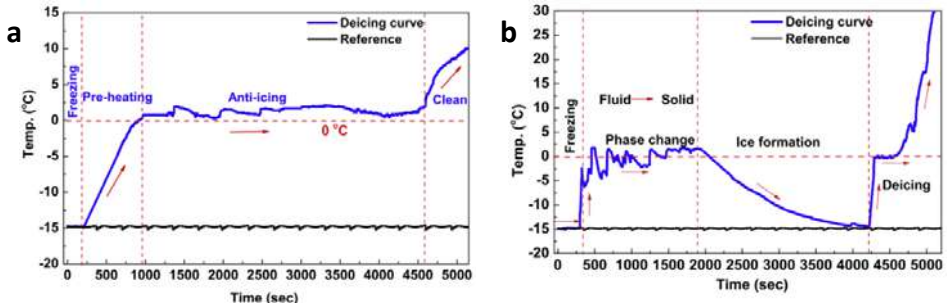

Figure 20 The deicing/anti-icing phenomenon of GPs-GE via. (a) anti-icing by pre-heating strategy under -15 °C temperature and 300 W/m^2 heat flux density; (b) ice formation under -15 °C followed by deicing with a heat flux density of 3000 W/m^2. (Figure adapted with permission from ref 129, Copyright 2017, Elsevier)

The anti-icing and deicing phenomenon demonstrate ice clean substrate with almost comparable energy consumption and are suitable for various structures according to the applications. For instance, anti-icing

phenomenon can be utilized for precautions against icing in cold humid conditions and deicing phenomenon for conditions to maintain ice clean surfaces.

Recent studies have also considered using 3D graphene foam (GrF) – polymer composites for deicing efficacy[130]. Bustillos et al. reported that polydimethylsiloxane (PDMS) based GrF exhibit superior deicing efficacy (477%) and electrical conductivity (500 Sm^{-1}) with only 0.1 vol. % of graphene as compared to other nanocarbon based deicing systems (2-100 vol% GNR exhibits 3-124 % efficacy). The time-dependent heating profiles (Figure 21) show the free-standing GrF-PDMS composite requires only 0.12 $W.cm^{-2}$ of power density to deice in 40 s. Whereas, GrF-PDMS composite coated in Ti-6Al-4V surface could deice the surface with 0.3 $W.cm^{-2}$ power density with a significant surface temperature difference of ~10 °C w.r.t free standing GrF-PDMS composite. Further, the volume concentration of graphene as foam in the deicing composite is 25 times lower than that of graphene based composites deicing systems with similar power density requirements[130].

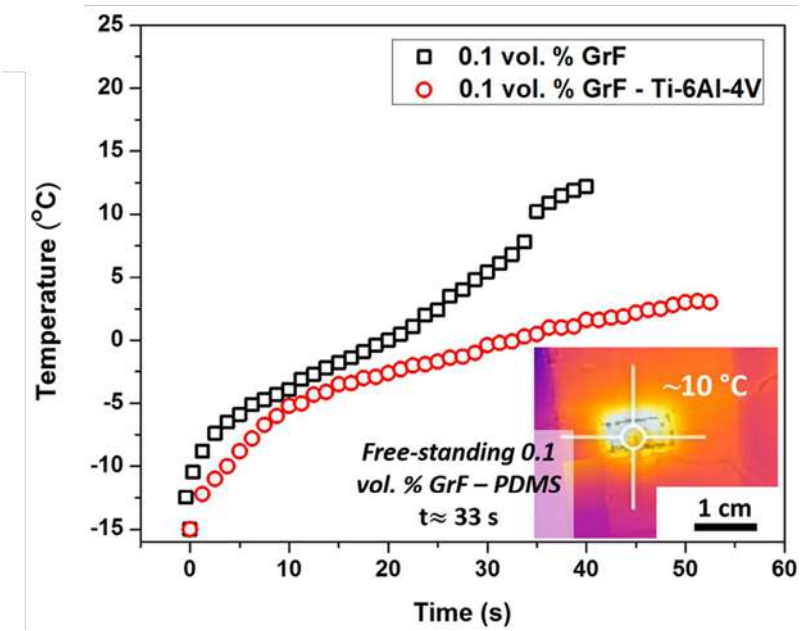

Figure 21 Heating profiles during deicing experiments of 0.1 vol. % GrF composites at 0.4 A current. Inset shows the thermal image of the composite during resistive heating. (Figure adapted with permission from ref 130)

Thus, the advanced graphene based composites exhibiting anti-icing and deicing characteristics which finds potential application as an intelligent engineering monitor and disaster-prevention in a low-temperature environment.

2.5 Investigation of self-cleaning/ oleophilic behavior

There has been a significant interest in research and commercial community to develop superhydrophobic materials that exhibit self-cleaning ability to shed fluids off the surfaces. Despite many applications of superhydrophobic coatings, they are essential as drag reduction coatings in the marine hull and as smart coatings in electronics. Superhydrophobic drag reduction coatings mitigate the skin friction drag, oxidation or corrosion on ship hulls and increase the fuel efficiency[131]. As a smart coating in flexible and wearable electronics, the self-cleaning mechanism prevents the malfunctioning of electronic devices triggered by water or chemical interaction[132]. For such superhydrophobic coatings, surface morphology plays a significant role in the wettability characteristics. By maintaining low surface energy and magnifying the surface roughness, the superhydrophobic state can be constructed. Similarly, superoleophilic materials can be constructed by increasing the surface roughness with slightly higher surface energy[133,134].

Recent studies have focused on the self-cleaning properties using graphene based materials. On deposition of graphene on a planar substrate, individual graphene sheets self-assemble to form an interconnected network. The resulting thin film of graphene increases the surface roughness of the substrate by one to two orders of magnitude[134]. Besides increasing the surface roughness, graphene in conjugation with other functional materials alter the surface chemistry and exhibit tuneable self-cleaning characteristics. Rafiee et al. established a facile technique to demonstrate a switchable surface characteristic by varying concentration ratio of volatile solvents[135]. A controllable contact angle (CA) ranging from 0° to 160° was displayed by the graphene surface. However, the switchable wettability characteristics is irreversible. Zhang et al. developed high adhesion graphene surfaces

which are highly hydrophobic and the switchable wettability characteristics which is reversible[136]. The adsorption and desorption of water molecules on the surface of graphene significantly controls the reversibility and this is achieved by using UV irradiation and air storage techniques. On exposure to UV light for 12 h, the CA of the film varied from 140° to 40°, demonstrating the transformation from hydrophobicity to hydrophilicity. The film reverted to hydrophobicity after air storage for 12 h.

Functionalisation is another efficient method to improve the wetting characteristics of graphene[137-139]. Lee et al. developed a transparent film of thermally reduced GO spheres which display CA of 125°. However, after functionalisation with silane, the CA reached 157° due to further lowering of the surface energy[140]. In another study, Zang et al. confirmed that apart from functionalisation of graphene, crumpling and unfolding a large area graphene sheet adhered to PDMS substrate resulted in hierarchical self-organization of graphene and tunable wettability[141]. Figure 22 illustrates the macroscopic deformation of a graphene sheet, microscopic structure, and wetting characteristics.

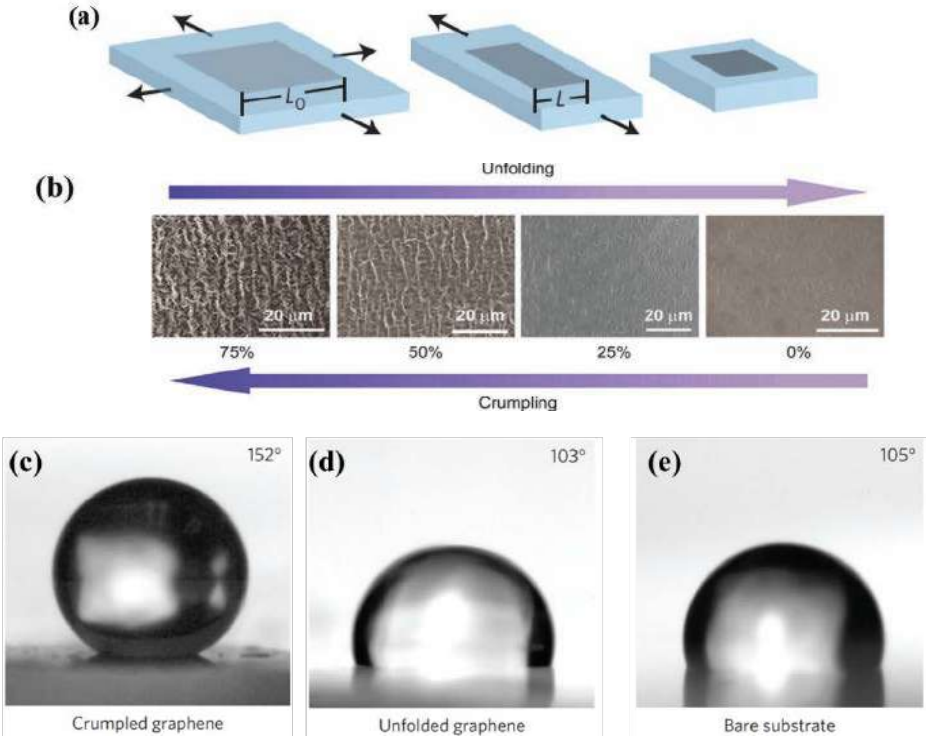

Figure 22. (a) Illustration of macroscopic deformation of a graphene sheet on a bi-axially pre-stretched substrate. (b) SEM micrograph of the graphene film at various strains (c-e) CA of a water droplet on crumpled, unfolded and bare graphene. (Figure adapted with permission from ref 141, Copyright 2013, Springer Nature)

A number of recent publications addressed on the fabrication of 3D graphene foams that exhibit superior superhydrophobic characteristics and superoleophilic over a broad range of oils and solvents. Interestingly, these materials exhibit good recyclability and excellent absorption characteristics[142]. Commercially available melamine sponge coated with graphene exhibited superhydrophobic and superoleophilic behavior[143]. The sponge displays CA of 162° and rapid absorbing capability of oils and solvents (Figure 23). Further, the density of oils and solvents influences the absorption capability of graphene sponges. The absorption capacity of graphene based sponges is 165 times its own weight which is significantly greater than that of nano-wire membranes (~20 times), microporous polymers (~33 times), and comparable to CNT sponges.

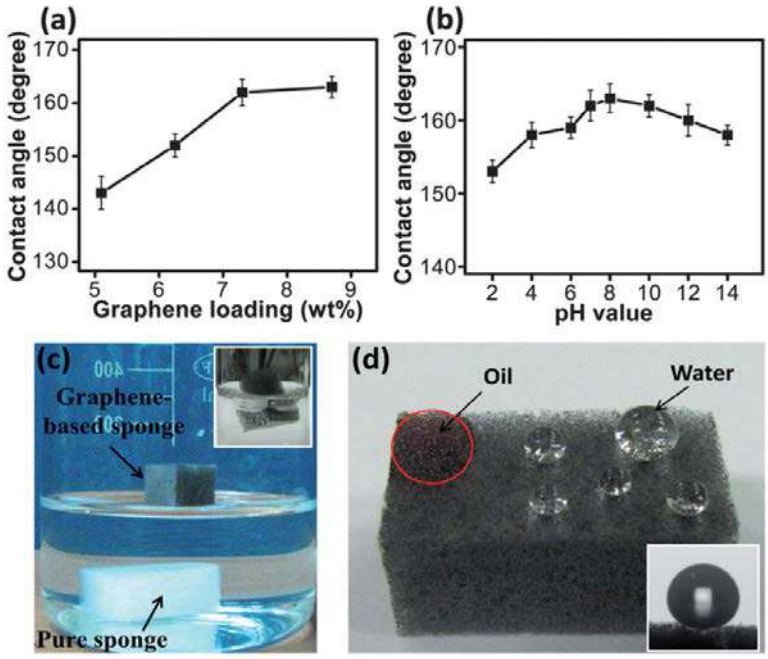

Figure 23 (a) Response of water CA due to graphene cocentration in sponges. (b) CA vs pH values of the graphene-based sponges. (c) Photo of graphene-based sponge floating in pure water. Inset shows graphene based foam immersed in water due to force. (d) Effect of water and oil droplets on the surface of the graphene based sponge. Inset shows water CA of 162°. (Figure adapted with permission from ref 143, Copyright 2008, RSC Publishing)

Further, spongy graphene also exhibits efficient absorption capability in toxic solvents and can be recycled by heat treatment resulting in full release of adsorbates[144].

Singh et al. reported teflon based graphene foams with superhydrophobic phenomenon at dynamic conditions. The advancing water CA is beyond 163°, while the receding CA is around 143°. Under dynamic impact test the CA on Teflon coated graphene foams stay persistent during the advancing and receding phases and finally the water droplet rebounds off the surface. However, on the pristine graphene foam, upon impact, the droplet pulsates and gets pinned on the surface[145] (shown in Figure 24). Such superhydrophobic surfaces finds potential application in marine structures where dynamic impact conditions are experienced.

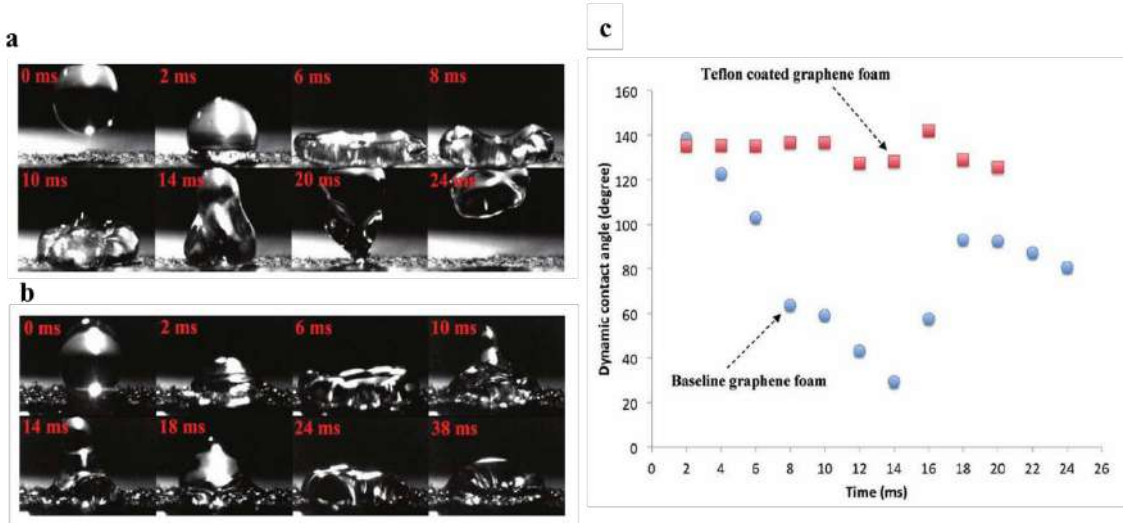

Figure 24. Snaps of a water droplet impacting (a) Teflon coated graphene foam. (b) graphene foam (c) Trend in contact angle on graphene foam and Teflon coated graphene foam under dynamic impact conditions. (Figure adapted with permission from ref 145, Copyright 2012, John Wiley and Sons)

Polymer-induced graphene composites exhibit enhanced superhydrophobicity in addition to good structural stability, cost-effectiveness and complementary functionalities. Hu et al. reported a ‘sticky’ superhydrophobicity

on a hybrid structure containing compressive graphene aerogels (CGA). This phenomenon is due to homogenous impregnation of PDMS along the cellular walls of CGA[146]. Pristine forms of CGA and PDMS exhibited a compromised hydrophobicity. But with an increase in PDMS concentration in the composite, superhydrophobicity was attained. The droplets on the composite exhibited strong adhesion behavior on the foam like structure (as shown in Figure 25). Further to unique wetting characteristics, these composite foams displayed significantly high compressibility and conductivity.

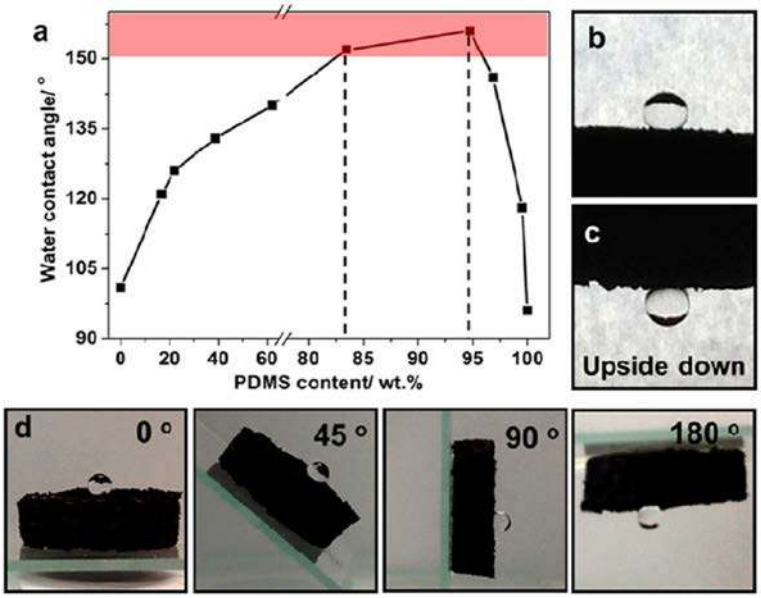

Figure 25 Superhydrophobic characteristics of PDMS/CGA. (a) Change in CA with respect to PDMS concentration. Shape of the water droplet on composite (b) up right position (c) upside-down (d) during rotation. (Figure adapted with permission from ref. 146)

Wang et al. developed a facile technique to synthesize electrochemically exfoliated graphene based PDMS coating that exhibited superhydrophobic behavior (CA 160°) showing robust resistance against water and sand impacts[147]. Similarly, rGO based diatomaceous earth modified PDMS based coatings exhibited robust superhydrophobicity with CA of 159°. Further, inclusions of TiO_2 improved CA to >170° due to the hierarchical surface roughness and excellent corrosion resistance and self-cleaning characteristics of TiO_2[148].

In another study, fluorinated GO (FGO) and PDMS based inks coated over a range of substrates exhibited superhydrophobic and oleophobic phenomenon. A water CA of 173.7° is attained with 60 wt% of FGO in PDMS. Such high CA is witnessed due to high surface roughness and reduced surface energy of the substrates[149]. Yang et al. developed epoxy based fluoro graphene coatings which exhibits stable superhydrophobic behavior (CA of 150°) sustaining 60 cycles of mechanical abrasions and excellent chemical stability in acidic and alkali mediums[150].

Zhu et al. integrated 3D graphene foams with a block copolymer of poly(2-vinylpyridene) and polyhexadecyl acrylate (P2VP-b-PHA), to exhibit switchable superoleophobic and superoleophilic phenomenon in response to pH medium[151]. The pH-responsive surfaces make good recyclability of oil/solvent adsorption and desorption. The composite foams could withstand 20 cycles of compressive stresses and gain weight of 40-196 times of its own weight.

Graphene based materials with superoleophilic characteristics can be used to address the adverse water pollution arising due to oil or chemical spillage. In principle, surfaces with superhydrophobic and superoleophilic phenomenon selectively absorb solvents and oils while being completely water repellent are preferred to address significant environmental issues such as oil spills in ocean, toxic solvent adsorption from industrial effluents etc.

2.6 Investigation of sensing properties

The growing interest in graphene is not only limited to its unusual physical properties but also extends to its electrical properties. The outstanding electrical properties of graphene is utilized in developing sensors for sensing strain, fatigue, toxic gases and chemicals, bacteria and biomolecules for food safety, toxic heavy metal ions, etc. The graphene based sensors when embedded with RFIDs, have the efficiency to revolutionize the Internet of Things (IoT).

Flexible and wearable graphene based strain sensors were prepared by adhering graphene woven fabric (GWF) on the polymer or medical tape composite films. Because of the crisscross configurations, the GWF possessed enormously high gauge factor, which is estimated to be ~ 10^3 under 2-6% strains, 10^6 under higher strains (>7%) and ~35 under the small strain of 0.2%. The signal from weak motions such as breathing, phonation, expression changes can be sensed (as shown in Figure 26). Further, it can sustain large distortion of 30% with entirely reversible electrical properties[152, 153].

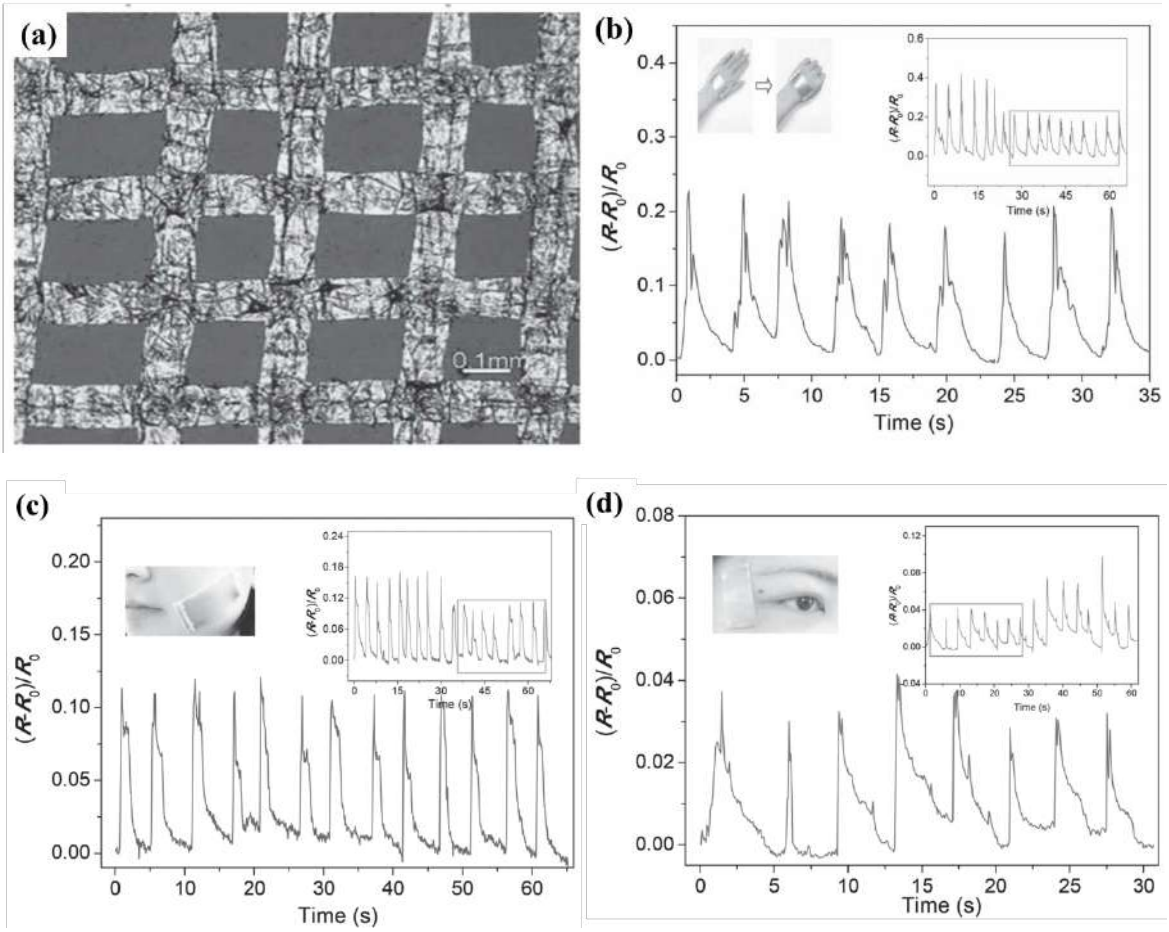

Figure 26 (a) Magnification of the optical image of the GWFs- PDMS composite film. Relative change of resistance during (b) hand motion (c) muscle motions in speech and (d) muscle motions of blinks. (Figure adapted with permission from ref 152, Copyright 2014, John Wiley and Sons)

In another study, hierarchically arranged thermally reduced graphene foams exhibited exceptional compression recovery property at strain levels up to 60%[154]. Under compressive deformation these foams exhibited reproducible change in resistance over 100 cycles. In addition, the foam based sensors can operate over temperature ranging from -50 ºC to 200 ºC resulting in gauge factors of 1.4, 1.3 and 1.4 at -50 ºC, 25 ºC and 200 ºC respectively (as shown in Figure 27). Such remarkable performance was not achieved with other carbon-based sensors.

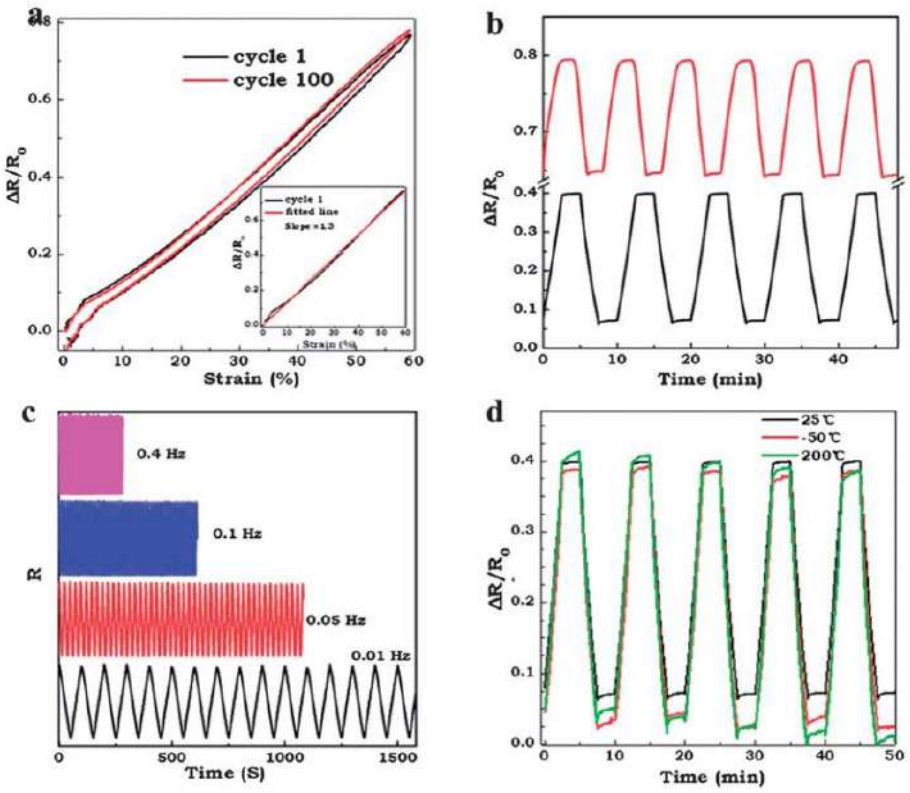

Figure 27. Piezoresistive behaviors of thermally reduced graphene foams. Relative resistance changes with applied compression strain (a) at cycle 1 and 100. (b) at compressive strains between 5% and 30%(black line) or 50% and 60% (red line) (c) at different frequencies and (d) at different temperatures (-50, 25, and 200 °C). (Figure adapted with permission from ref 154, Copyright 2013, RSC Pub)

Effective conductive pathways were obtained in polymer composites of graphene/ thermoplastic polyurethane (TPU) foams and TPU/CNT/graphene nanocomposites which finds potential application in structural health monitoring[155]. Some of the graphene based elastomer composites exhibit excellent strain sensing efficacies. Boland et al. fabricated graphene based elastomer conducting composites which display increased strain sensing properties and operates at strains greater than 800%. These composites exhibit gauge factor up to 35 and the sensitivity remains undiminished up to 160Hz vibrational frequency under dynamic strains[156]. In another study, Lin et al. fabricated graphene/natural rubber (NRGE) composite with staggered nanostructured graphene network by novel ice-templating strategy (Figure 28). The resulting composite containing 0.42 vol% of graphene exhibited high sensitivity, stretchability, and reproducibility up to ~400 cycles with 60% of strain[157].

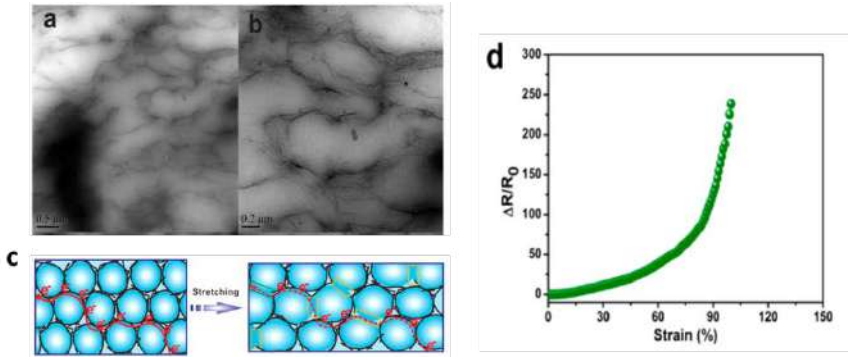

Figure 28 (a, b) TEM of segregated composites (c) Representation of conductive network evolution in the composites. NR phase is denoted by blue circles, the conductive network by the black lines, and electrons by red e- (d) Relative change in resistance as a function of applied strain. (Figure adapted with permission from ref. 157)

In addition to motion monitoring and strains sensing efficacies, graphene has shown promising bio-sensing, heavy metal ion, toxic gas sensing capabilities[158]. The mechanism of detection is mainly focused on the variation of conductance upon the adsorption of the sensing element. The adsorption of electron donating species such as NH_3

de-dope the graphene and results in reduced conductance. Whereas, the adsorption of electron withdrawing species such as NO_2 enhances the doping level in graphene and results in increased conductance.

Recently, researchers have developed a stretchable, flexible and wearable sensor based on the Internet of Technology (IoT)[159,160]. 3D graphene foam/PDMS composite was constructed as an armband measurement device to track gestures and fitness. The data measured by the sensor is transferred via WiFi and displayed on a website. Such an advancement can provide numerous applications with battery-free wireless monitoring devices in the inaccessible region to sense moisture, toxic chemicals or gases, radiations, and nuclear wastes.

2.7 Investigation of flame retardant properties

Graphene and its derivatives are active in altering the polymeric combustion cycle by modifying pyrolysis, heat absorption, thermal conductivity, and dripping characteristics of flame retarded polymers[161]. Graphene based derivatives are capable of exhibiting flame retardant mechanism by formation of dense, coherent char layer on interaction with a heat source. The char layer functions as a barrier layer limiting the heat transmission from the ignition source and mitigating the diffusion of pyrolysed products from the polymer substrate. Thus, graphene and its derivatives function as a template substrate for the char growth, by encouraging the formation of multiple and overlapped, stable and protective carbonaceous residual layers[162-165].

Graphene in combination with inorganic nanoparticles resulted in significant enhancements in flame retardancy properties. Graphene nanosheets decorated with ferrocene particles[166], aluminium[167] and cobalt[168] nanoparticles resulted in improved flame retardancy characteristic in polymer composites. The flame retardancy characteristics of the composites is ascribed to (i) indirect diffusion path generated by the graphene, (ii) catalyst phenomenon of the inorganic nanoparticles towards the char formation, (iii) the adsorption capability of the graphene and (iv) the combined efficiency of graphene and the decorated metal oxide.

Han et al. prepared composites of polystyrene incorporated with thermally reduced graphene oxides of varying reduction rates[169]. The different degree of reduction temperature resulted in graphene with varying structure and morphology. It is witnessed that at high reduction temperature (800 ^oC) the graphene sheets are highly expanded and disordered. This highly reduced graphene reinforced composites demonstrated 47.5% decrease in peak heat release rate, thus representing the flame retardant characteristics is strongly dependent on the degree of reduction and morphology of graphene.

Liu et al. evaluated the flame retardant properties of epoxy systems reinforced with graphene and layered hydroxide and phosphorous based flame retardants. With addition of 2.5 wt% of graphene and phosphorous based flame retardant, the epoxy system exhibits enhanced flame retardancy by mitigating the dripping phenomenon, total heat release, peak heat release rate and increasing the limiting oxygen index[170]. Standard flame retardant composites require 1.1 to 7.8 wt% of phosphorous, however in presence of graphene low concentration of phosphorous was sufficient to exhibit the flame retardant property[171].

Thus ease of processability of graphene and its derivatives in combination with range of polymers has resulted in the development of advanced flame retardant materials which is suitable for electronic enclosures, technical textiles and composites for engineering applications. Further replacing halogenated flame retardant with graphene can result in the development of environment friendly products. However, there is a significant lack of data on the influence of organic products, toxic effluents which are formed due to exposure to flame and the degree of toxicity on the human body.

3. Conclusions and Perspectives

It has been resolved from the entire disclosure that graphene has the power to alter the material properties which are suitable for harsh environments. By combining the outstanding properties of graphene with polymer, a number of noble materials can be realized. We have summarised the properties of graphene which are suitable for harsh environments. Furthermore, the characteristics of graphene based composites in harsh operational conditions, such as cryo-mechanical properties, ballistic impact resistance, thermal conductivity, deicing/anti-icing behavior, self-cleaning and sensing properties have been discussed. The performance efficiency of graphene based composites is primarily based on the availability of graphene which completely relies on efficient composites preparation techniques. Also, it is evident that the design of graphene fillers within the composite has a significant impact on their performance. For instance, the homogenous dispersion of graphene and the molecular interaction between filler and the host matrix play a substantial role in improving the mechanical properties of composites. Alignment of graphene within the host matrix has significantly improved the performance in terms of self-cleaning and deicing capabilities, thermal conductivity and better sensing stability. Experimental evidence shows the opportunity of graphene composites to be explored in harsh operating conditions, however a comprehensive study on their mechanism in these conditions is still required to tailor their properties.

Despite these pros, which explain the increasing interest in academic and industrial world towards the enhancement of graphene based composite capable of operating in harsh conditions, some challenging issues still persist and have to be overcome.

- Firstly, although graphene demonstrates outstanding properties, it is not facile to develop graphene based composites in a controllable manner to exhibit consistent performance in harsh operating conditions. Hence controllable dispersion and modification of graphene have been recommended to overcome this problem.
- Further, in the composite systems, there are some factors which are obviously responsible their performance in harsh operating conditions.
  (i) Aggregation prevention of graphene during the processing of composites.
  (ii) Strong interface between the graphene and the polymeric phase
  (iii) Alignment of graphene within graphene within the host system
- A broad study on the performance of graphene based composites in harsh operating conditions is still inadequate and involves sophisticated characterization tools which can simulate operating conditions such as extreme temperature conditions, excessive shear, vibrations, electromagnetic interfaces, radiations and many more.
- Cognitive computing technology and IoT being the fast-growing segments of technology. In near future it is very probable to develop smart graphene composite devices with inter-disciplinary collaboration for intelligent engineering systems.
- In addition to experimental investigations, the numerical analysis and simulation information regarding the change of properties in various service environments is still inadequate. Methods and simulation techniques need to develop to understand their performance, as well as the transformation in the property with respect to time parameter, has to be considered.

Acknowledgments

This project was funded by the research grant from the Swinburne University of Technology (SUPRA). We acknowledge support from the Australian Research Council (ARC) for the DECRA fellowship for N.H. (DE170101249) and the Centre of Surface Engineering for Advanced Materials, SEAM, which has been funded under the ARC Industrial Transformation Training Centre (ITTC) scheme via Award IC180100005.

References

(1) Balint, T. S.; Kolawa, E. A.; Cutts, J. A.; Peterson, C. E. Extreme Environment Technologies for NASA's Robotic Planetary Exploration. *Acta Astronaut.* **2008**, *63*, 285.

(2) Zeitlin, C.; Hassler, D.M.; Cucinotta, F.A.; Ehresmann, B.; Wimmer-Schweingruber, R.F.; Brinza, D.E.; Kang, S.; Weigle, G.; Böttcher, S.; Böhm, E.; Burmeister, S.; Guo, J.; Köhler, J.; Martin, C.; Posner, A.; Rafkin, S.; Reitz, G. Measurement of Energetic Particle Radiation in Transit to Mars on the Mars Science Laboratory. *Science* **2013**, *340,* 1080.

(3) Mangolini, F.; Krick, B. A.; Jacobs, T.D.B.; Khanal, S.R.; Streller, F.; McClimon, J.B.; Hilbert, J.; Prasad, S.V.; Scharf, T.W.; Ohlhausen, J.A.; Lukes, J.R.; Sawyer, W.G.; Carpick, R.W. Effect of silicon and oxygen dopants on the stability of hydrogenated amorphous carbon under harsh environmental conditions. *Carbon* **2018**, *130*, 127.

(4) Kawai, M.; Yagihashi, Y.; Hoshi, H.; Iwahori, Y. Anisomorphic constant fatigue life diagrams for quais-isotropic woven fabric carbon/epoxy laminates under different hygro-thermal environments. *Adv. Comp. Mat.* **2013**, *22*, 79.

(5) Dai, K.; Bergot, A.; Liang, C.; Xiang, W.N.; Huang, Z. Environmental issues associated with wind energy – A review. *Renew. Ene.* **2015**, *75*, 911.

(6) Zinkle, S.J.; Was, G.S. Materials challenges in nuclear energy. *Acta Mat.* **2013**, *61*, 735

(7) Wu, J.; Yuan, X.Z.; Martin, J.J.; Wang, H.; Zhang, J.; Shen, J.; Wu, S.; Merida, W. A review of PEM fuel cell durability: Degradation mechanisms and mitigation strategies. *J. Power Sources* **2008**, *184*, 104

(8) Latourte, F.; Wei, X.; Feinberg, Z.D.; Vaucorbeil, A.; Tran, P.; Olson, G.B.; Espinosa, H.D. Design and identification of high performance steel alloys for structures subjected to underwater impulsive loading. *Int. J. Solid Struct.* **2012**, *49*, 1573.

(9) https://www.compositesworld.com/articles/nasaboeing-composite-launch-vehicle-fuel-tank-scores-firsts

(10) Wang, J.; Zhou, Q.; Chao, D.; Li, F.; Cui, T. In situ determination of mechanical properties for poly(ether ether ketone) film under extreme conditions. *RSC. Adv.* **2017**, *7*, 8670.

(11) Gabrion, X.; Placet, V.; Trivaudey, F.; Boubakar, L. About the thermomechanical behaviour of a carbon fibre reinforced high-temperature thermoplastic composite. *Compos. Part B-Eng.* **2016**, *95*, 386.

(12) Correia, J. R.; Gomes, M. M.; Pires, J.M.; Branco, F.A. Mechanical behaviour of pultruded glass fibre reinforced polymer composites at elevated temperature: Experiments and model assessment. *Compos. Struct.* **2013**, *98*, 303.

(13) Mallick, P.K. *Fiber-reinforced composites: materials, manufacturing, and design*; CRC Press, 2007.

(14) Ajayan, P. M.; Schadler, L. S.; Braun, P. V. *Nanocomposite science and technology*; Wiley-VCH: Morlenbach, 2005.

(15) Vaia, R. A.; Price, G.; Ruth, P.N.; Nguyen, H. T.; Lichtenhan, J. Polymer/layered silicate nanocomposites as high performance ablative materials. *Appl. Clay Sci.* **1999**, *15*, 67.

(16) Gilman, J.W.; Jackson, C.L.; Morgan, A.B.; Harris, R. Flammability Properties of Polymer−Layered-Silicate Nanocomposites. Polypropylene and Polystyrene Nanocomposites. *Chem. Mater.* **2000**, *12*, 1866.

(17) Wang, L.; Han, D.; Luo, J.; Li, T.; Lin, Z.; Yao, Y. Highly Efficient Growth of Boron Nitride Nanotubes and the Thermal Conductivity of Their Polymer Composites. *J. Phys. Chem. C* **2018**, *122*, 1867.

(18) Amirsardari, Z.; Aghdam, R.M.; Niasari, M.S.; Shakhesi, S. Preparation and characterization of nanoscale ZrB2/carbon–resol composite for protection against high-temperature corrosion. *J. Therm. Anal. Calorim.* **2015**, *120*, 1535.

(19) Zeng, X.Y.; Zhang, Q.K.; Yu, R.M.; Lu, C.Z. A New Transparent Conductor: Silver Nanowire Film Buried at the Surface of a Transparent Polymer. *Adv. Mater.* **2010**, *22*, 4484.

(20) Lee, J.; Lee, P.; Lee, H.B.; Hong, S.; Lee, I.; Yeo, J. ; Lee, S.S.; Kim, T.S.; Lee, D.; Ko, S.H. Room-Temperature Nanosoldering of a Very Long Metal Nanowire Network by Conducting-Polymer-Assisted Joining for a Flexible Touch-Panel Application. *Adv. Mater.* **2013**, *23*, 4171.

(21) Rodriguez, A.J.; Guzman, M.E.; Lim, C.S.; Minaie, B. Mechanical properties of carbon nanofiber/fiber-reinforced hierarchical polymer composites manufactured with multiscale-reinforcement fabrics. *Carbon* **2011**, *49*, 937.

(22) Yang, S.; Lozano, K.; Lomeli, A.; Foltz, H. D.; Jones, R. Electromagnetic interference shielding effectiveness of carbon nanofiber/LCP composites. *Compos. Part A-Appl. Sci. Manf.* **2005**, *36*, 691.

(23) Ji1, S.; Hyun, B.G.; Kim, K.; Lee, S.Y.; Kim, S.H.; Kim, J.Y.; Song, M.H.; Park, J.U. Photo-patternable and transparent films using cellulose nanofibers for stretchable origami electronics. *NPG Asia Mater.* **2016**, *8.*

(24) Chen, Y.; Zhang, H.B.; Yang, Y.; Wang, M.; Cao, A.; Yu, Z.Z. High-Performance Epoxy Nanocomposites Reinforced with Three-Dimensional Carbon Nanotube Sponge for Electromagnetic Interference Shielding. *Adv. Funct. Mater.* **2016**, *26*, 447

(25) Li, Z.; Liang, Z. Optimization of Buckypaper-enhanced Multifunctional Thermoplastic Composites. *Sci. Rep.* **2017**, *7*, 42423.

(26) Choi, E.Y.; Kim, K.; Kim, C.K.; Kang, E. Reinforcement of nylon 6,6/nylon 6,6 grafted nanodiamond composites by in situ reactive extrusion. *Sci. Rep.* **2016**, *6*, 37010.

(27) Hameed, N.; Dumée, L.F.; Allioux, F.M.; Reghat, M.; Church, J.S.; Naebe, M.; Magniez, K.; Parameswaranpillai, J.; Fox, B.L. Graphene based room temperature flexible nanocomposites from permanently cross-linked networks. *Sci. Rep.* **2018**, *8*, 2803.

(28) Martino, L.; Guigo, N.; Berkel, J.G.; Sbirrazzuoli, N. Influence of organically modified montmorillonite and sepiolite clays on the physical properties of bio-based poly(ethylene 2,5-furandicarboxylate). *Compos. Part-B-Eng.* **2017**, *110*, 96

(29) Zabihi, O.; Ahmadi, M.; Nikafshar, S.; Preyeswary, K.C.; Naebe, M. A technical review on epoxy-clay nanocomposites: Structure, properties, and their applications in fiber reinforced composites. *Compos. Part-B-Eng.* **2017**, *135*, 1.

(30) Guo, T.; Heng, L.; Wang, M.; Wang, J.; Jiang, L. Robust Underwater Oil-Repellent Material Inspired by Columnar Nacre. *Adv. Mater.* **2016**, *28*, 8505.

(31) Auto applications of drive commercialization of nanocomposites. *Plastic Additives & Compounding* **2002**, *4*, 30.

(32) Patterson, T., Forte™ nanocomposites – our revolutionary breakthrough. 4th World Congress in Nanocomposites, EMC, San Francisco, 1-3 September 2004.

(33) Goldman, A. Y. Multilayer barrier liner material with nanocomposites for packaging applications. 4th World Congress in Nanocomposites, EMC, San Francisco, 1-3 September 2004.

(34) Nesher, G.; Aylien, M.; Sansaki, G.; Anvir, D.; Marom, G. Polyaniline Entrapped in Silver: Structural Properties and Electrical Conductivity. *Adv. Func. Mater.* **2009**, *19*, 1293.

(35) Rong, M.Z.; Zhang, M.Q.; Wang, H.B.; Zeng, H.M. Surface modification of magnetic metal nanoparticles and its influence on the performance of polymer composites. *J. Polym. Sci.* **2003**, *41*, 1070.

(36) Li, P.; Liu, W.; Dennis, J.S.; Zeng, H.C. Ultrafine Alloy Nanoparticles Converted from 2D Intercalated Coordination Polymers for Catalytic Application. *Adv. Func. Mater.* **2016**, *26*, 5658.

(37) Elbahri, M.; Homaeigohar, S.; Abdelaizz, R.; Dai, T.; Khalil, R.; Zillohu, A.U. Smart Metal–Polymer Bionanocomposites as Omnidirectional Plasmonic Black Absorber Formed by Nanofluid Filtration. *Adv. Func. Mater.* **2012**, *22*, 4771.

(38) Jalali, M.; Dauterstedt, S.; Michaud, A.; Wuthrich, R. Electromagnetic shielding of polymer–matrix composites with metallic nanoparticles. *Compos. Part B-Eng.* **2011**, *42*, 1420.

(39) Singh, P.K.; Sharma, K.; Kumar, A.; Shukla, M. Effects of functionalization on the mechanical properties of multiwalled carbon nanotubes: A molecular dynamics approach. *J. Compos. Mater.* **2016**, *51*, 1.

(40) Endo, M.; Noguchi, T.; Ito, M.; Takeuchi, K.; Hayashi, T.; Kim, T. Wanibuchi, H. Jinnai, M. Terrones, M. S. Dresselhaus, Extreme-performance Rubber Nanocomposites for Proving and Excavating Deep Oil Resources Using Multi-walled Carbon Nanotubes. Adv. Func. Mat. 18 (2008) 3403.

(41)Kumar, A.; Shrama, K.; Dixit, A.R. A review of the mechanical and thermal properties of graphene and its hybrid polymer nanocomposites for structural applications. *J. Mater. Sci.* **2019**, *54*, 5992.

(42) Potts, J.R.; Dreyer, D.R.; Bielawski, C.W.; Ruoff, R.S. Graphene-based polymer nanocomposites. *Polymer* **2011**, *52*, 5.

(43) Geim, A.K.; Novoselov, K.S. The rise of graphene. *Nat. Mater.* **2007**, *6*, 183.

(44) Ghany, N.A.A.; Elsherif, S. A.; Handal. H. T. Revolution of graphene for different applications: state-of-the-art. *Surf. and Interf.* **2017**, *9*, 93.

(45) Geim, A.K. Graphene: status and prospects. *Science* **2009**, *324*, 1530.

(46) Novoselov, K.S.; Geim, K.S.; Morozov, S. V.; Jiang, D.; Katsnelson, M.I.; Grigorieva, I. V.; Dubonos, S. V.; Firsov, A.A. Two-dimensional gas of massless Dirac fermions in graphene. *Nature* **2005**, *438*, 197.

(47) Fasolino, A.; Los, J.H.; Katsnelson, M.I. Intrinsic ripples in graphene. *Nat. Mater.* **2007**, *6*, 858.

(48) Lee, C.; Wei, X.; Kysar, J.W.; Hone, J. Measurement of the elastic properties and intrinsic strength of monolayer graphene. *Science* **2008**, *321*, 80.

(49) Scarpa, F.; Adhikari, S.; Phani, A.S. Effective elastic mechanical properties of single layer graphene sheets. *Nanotechnology* **2009**, *20*, 65709.

(50) Vidu, R.; Rahman, M.; Mahmoudi, M.; Enachescu, M.; Poteca, T.D. Nanostructures: a platform for brain repair and augmentation. *I. Opris, Front. Syst. Neurosci.* **2014**, *8*, 91.

(51) Phiri, J.; Gane, P.; Maloney, T.C. General overview of graphene: production, properties and application in polymer composites. *Mater. Sci. Eng. B.* **2017**, *215*, 9.

(52) Chen, H.; Muller, M.B.; Gilmore, K.J.; Wallace, G.G.; Li, D. Mechanically Strong, Electrically Conductive, and Biocompatible Graphene Paper. *Adv. Mater.* **2008**, *20*, 3557.

(53) Lee, C.; Wei, X.; Kysar, J.W.; Hone, J. Measurement of the Elastic Properties and Intrinsic Strength of Monolayer Graphene, *Science* **2008**, *18*, 385.

(54) Papageorgiou, D.G.; Kinloch I.A.;Young, R.A. Mechanical properties of graphene and graphene-based nanocomposites. *Prog. Mater. Sci.* **2017**, *90*, 75.

(55) Frank, I.W.; Tanebaum, D.M.; Zande, A.M.; McEuen, P.L. Mechanical properties of suspended graphene sheets. *J. Vac. Sci. Tech. B* **2007**, *25*, 2558.

(56) Lee, J.H.; Loya, P.E.; Lou, J.; Thomas, E.L. Dynamic mechanical behaviour of multilayer graphene via. supersonic projectile penetration. *Science* **2014**, *28*, 1092.

(57) Min, K.; Aluru, N.R. Mechanical properties of graphene under shear deformation. *Appl. Phys. Lett.* **2011**, *98*, 013113.

(58) Balandin, A.A.; Ghosh, S.; Bao, W.; Calizo, I.; Teweldebrhan, D.; Miao, F.; Lau, C.N. Superior thermal conductivity of single-layer graphene. *Nano Letters* **2008**, *8*, 902.

(59) Ghosh, S.; Calizo, I.; Teweldebrhan, D.; Pokatilov, E. P.; Nika, D. L.; Balandin, A. A.; Bao, W.; Miao, F.; Lau, C. N. Extremely high thermal conductivity of graphene: Prospects for thermal management applications in nanoelectronic circuits. *Appl. Phys. Lett.* **2008**, *92*, 151911

(60) Ghosh, S.; Bao, W.; Nika, D.L.; Subrina, S.; Pokatilov, E.P.; Lau, C.N.; Balandin, A.A. Dimensional crossover of thermal transport in few-layer graphene. *Nat. Mat.* **2010**, *9*, 555.

(61) Bae, M.H.; Li, Z.; Aksamija, Z.; Martin, P.N.; Xiong, F.; Ong, Z.Y.; Knezevic, I.; Pop, E. Ballistic to diffusive crossover of heat flow in graphene ribbons. *Nat. Comm.* **2013**, *4,* 1.

(62) Varshney, V.; Patnaik, S.S.; Roy, A.K.; Froudakis, G.; Farmer, B.L. Modeling of Thermal Transport in Pillared-Graphene Architectures. *ACS Nano* **2010**, *4*, 1153.

(63) Yao, W.; Cao, B.Y.; Thermal wave propagation in graphene studied by molecular dynamics simulations, *Chin. Sci. Bull.* **2014**, *59*, 3495.

(64) Shahil, K.M.F.; Balandin, A.A. Graphene–Multilayer Graphene Nanocomposites as Highly Efficient Thermal Interface Materials. *Nano Lett.* **2012**, *12*, 861.

(65) Han, Z.; Fina, A. Thermal Conductivity of Carbon Nanotubes and Their Polymer Nanocomposites: A Review. *Prog. Polym. Sci.* **2011**, *36*, 914.

(66) Teng, C.C.; Ma, C.M.; Lu, C.; Yang, S.; Lee, S.; Hsiao, M.; Yen, M.; Chiou, K.; Lee, T. Thermal conductivity and structure of non-covalent functionalized graphene/epoxy composites. *Carbon* **2011**, *49*, 5107.

(67) Yu, A.; Ramesh, P.; Sun, X.; Bekyarova, E.; Itkis, M.E.; Haddon, R.C. Enhanced Thermal Conductivity in a Hybrid Graphite Nanoplatelet – Carbon Nanotube Filler for Epoxy Composites. *Adv. Mater.* **2008**, 20, 4740.

(68) Cao, M.S.; Wang, X.X.; Cao, W.Q. Ultrathin graphene: electrical properties and highly efficient electromagnetic interference shielding. *J. Mater. Chem. C* **2015**, *3*, 6589.

(69) Marsden, A.J.; Papageorgiou, D.G.; Valles, C.; Liscio, A.; Palermo, V.; Bissett, M.A.; Young, R.J.; Kinloch I.A. Electrical percolation in graphene–polymer composites. *2D Mater.* **2018**, *5*, 1.

(70) Hong, S.K.; Kim, K.Y.; Kim, T.Y.; Kim, J.H.; Park, S.W.; Kim, J.H.; Cho, B.J. Electromagnetic interference shielding effectiveness of monolayer graphene. *Nanotechnology* **2012**, *23*, 1.

(71) Wu, D.; Zhang, F.; Liang, H.; Feng, X. Nanocomposites and macroscopic materials: assembly of chemically modified graphene sheets. *Chem. Soc. Rev.* **2012**, *41*, 6160.

(72) Xu, Z.; Gao, C. Graphene chiral liquid crystals and macroscopic assembled fibres. *Nat. Commun.* **2011**, *571*, 1.

(73) Xin, G.; Yao, T.; Sun, H.; Scott, S.M.; Shao, D.; Wang, G.; Lian, J. Highly thermally conductive and mechanically strong graphene fibers. *Science* **2015**, *349*, 1083.

(74) Chen, H.; Muller, M.B.; Gilmore, K.J.; Wallace, G.G.; Li, D. Mechanically strong, electrically conductive and biocompatible graphene paper. *Adv. Mater.* **2008**, *20*, 3557.

(75) Tung, V.C.; Allen, M.J.; Yang, Y.; Kaner, R.B. High-throughput solution processing of large-scale graphene. *Nat. Nanotechnol.* **2009**, *4*, 25.

(76) An, S.J.; Zhu, Y.; Lee, S.H.; Stoller, M.D.; Emilsson, T.; Park, S.; Velamakanni, A.; An, J.; Ruoff, R.S. Thin Film Fabrication and Simultaneous Anodic Reduction of Deposited Graphene Oxide Platelets by Electrophoretic Deposition. *J. Phys. Chem. Lett.* **2010**, *1*,1259.

(77) Xin, G.; Sun, H.; Hu, T.; Fard, H.R.; Sun, X.; Koratkar, N.; Borca-Tascius, T.; Lian, J. Large-Area Freestanding Graphene Paper for Superior Thermal Management. *Adv. Mater.* **2014**, *26*, 4521.

(78) Chen, Z.; Ran, W.; Gao, L.; Liu, B.; Pai, S.; Cheng, H.M. Three-dimensional flexible and conductive interconnected graphene networks grown by chemical vapour deposition. *Nat. Mater.* **2011**, *10*, 424.

(79) Zhao, Y.; Liu, J.; Hu, Y.; Cheng, H.; Hu, C.; Jiang, C.; Jiang, L.; Cao, A.; Qu, L. Highly Compression-Tolerant Supercapacitor Based on Polypyrrole-mediated Graphene Foam Electrodes. *Adv. Mater.* **2012**, *4*, 591.

(80) Xu, L.; Sheng, K.; Li, C.; Shi, G. Self-Assembled Graphene Hydrogel via a One-Step Hydrothermal Process. *ACS Nano.* **2010**, *4*, 4324.

(81) Sun, H.; Xu, Z.; Gao, C. Multifunctional, Ultra-Flyweight, Synergistically Assembled Carbon Aerogels. *Adv. Mater.* **2013**, *25*, 2554.

(82) Shen, K.; Sun, Y.; Li, C.; Yuan, W.; Shi, G. Ultrahigh-rate supercapacitors based on eletrochemically reduced graphene oxide for ac line-filtering. *Sci. Rep.* **2012**, *2*, 247.

(83) Wu, C.; Huang, X.; Wu, X.; Qian, R.; Jiang, P. Mechanically flexible and multifunctional polymer-based graphene foams for elastic conductors and oil water separators. *Adv. Mater.* **2013**, *39*, 5658.

(84) Shen, X.J.; Liu, Y.; Xiao, H.M.; Feng, Q.P.; Yu, Z.Z.; Fu, S.Y. The reinforcing effect of graphene nanosheets on the cryogenic mechanical properties of epoxy resins. *Compos. Sci. Technol.* **2012**, *13*, 1581.

(85) Chen, Z.K.; Yang, J.P.; Ni, Q.Q.; Fu, S.Y.; Huang, Y.G. Reinforcement of epoxy resins with multi-walled carbon nanotubes for enhancing cryogenic mechanical properties. *Polymer* **2009**, *50*, 4753.

(86) Shao, Y.; Xu, F.; Liu, W.; Zhou, M.; Li, W.; Hui, D.; Qiu, Y. Influence of cryogenic treatment on mechanical and interfacial properties of carbon nanotube fiber/bisphenol-F epoxy composite. *Compos. Part B-Eng.* **2017**, 125, 195.

(87) Hussein, A.; Sarkar, S.; Lee, K.; Kim, B. Cryogenic fracture behavior of epoxy reinforced by a novel graphene oxide/poly(p-phenylenediamine) hybrid, *Compos. Part B-Eng.* **2017**, *129*, 133.

(88) Wu, Y.; Chen, M.; Chen, M.; Ran, Z.; Zhu, C.; Liao, H. The reinforcing effect of polydopamine functionalized graphene nanoplatelets on the mechanical properties of epoxy resins at cryogenic temperature. *Polym. Test.* **2017**, *58*, 262.

(89) Shen, X.J.; Meng, L.X.; Yan, Z.Y.; Sun, C.J.; Ji, Y.H.; Xiao, H.M.; Fu, S.Y. Improved cryogenic interlaminar shear strength of glass fabric/epoxy composites by graphene oxide, *Compos. Part B-Eng.* **2015**, *73*, 126.

(90) Wu, Z.; Li, J.; Huang, C.; Li, L. Effect of matrix modification on interlaminar shear strength of glass fibre reinforced epoxy composites at cryogenic temperature. *Phys. Pro.* **2015**, *67*, 1068.

(91) Li, F.; Hua, Y.; Qu, C.B.; Xiao, H.M.; Fu, S.Y. Greatly enhanced cryogenic mechanical properties of short carbon fiber/polyethersulfone composites by graphene oxide coating. *Compos. Part A-App. Sci. Manuf.* **2016**, *89*, 47.

(92) Ghosh, S.K.; Rajesh, P.; Srikavya, B.; Rathore, D.K.; Prusty, R.K.; Ray, B.C. Creep behavior prediction of multi-layer graphene embedded glass fiber/epoxy composites using time-temperature superposition principle. *Compos. Part A-App. Sci. Manuf.* **2018**, *107*, 507.

(93) Jiang, T.; Kuila, T.; Kim, N.H.; Lee, J.H. Effects of surface-modified silica nanoparticles attached graphene oxide using isocyanate-terminated flexible polymer chains on the mechanical properties of epoxy composites. *J. Mater. Chem. A* **2014**, *2*, 10557.

(94) Ozden, S.; Machado, L.D.; Tiwary, C.; Autreto, P.A.; Vajtai, R.; Barrera, E.V.; Galvao, D.S.; Ajayan, P.M. Ballistic Fracturing of Carbon Nanotubes. *ACS Appl. Mater. Inter.* **2016**, *8*, 24819.

(95) O'Masta, M.R.; Russell, B.P.; Deshpande, V.S. An Exploration of the Ballistic Resistance of Multilayer Graphene Polymer Composites. *Ext. Mech. Lett.* **2017**, *11*, 49.

(96) Kausar, A.; Rafique, I.; Anwar, Z.; Muhammad, B. Perspectives of Epoxy/Graphene Oxide Composite: Significant Features and Technical Applications. *Polym. – Plast. Tech. Eng.* **2016**, *55*, 704.

(97) Qi, B.; Yu, J. Enhanced thermal and mechanical properties of epoxy composites by mixing thermotropic liquid crystalline epoxy grafted graphene oxide. *express Polym. Lett.* **2014**, *8*, 467.

(98) Rafiq, R.; Cai, D.; Jin, J.; Song, M. Increasing the Toughness of Nylon 12 by the Incorporation of Functionalized Graphene, *Carbon* **2010**, *48*, 4309.

(99) Pedrazzoli, D.; Pegoretti, A.; Kalaitzidou, K. Synergistic effect of exfoliated graphite nanoplatelets and short glass fiber on the mechanical and interfacial properties of epoxy composites. *Compos. Sci. Tech.* **2014**, *98*, 15.

(100) Bulut, M. Mechanical characterization of Basalt/epoxy composite laminates containing graphene nanopellets. *Compos. Part B- Eng.* **2017**, *122*, 71.

(101) Avila, A.F.; Neto, A.S.; Junior, H.N. Hybrid Nanocomposites for Mid-Range Ballistic Protection. *Int. J. Impact Eng.* **2011**, *38*, 669.

(102) Shanker, A.; Li, C.; Kim, G.H.; Gidley, D.; Pipe, K.P.; Kim, J. High thermal conductivity in electrostatically engineered amorphous polymers. *Sci. Adv.* **2017**, *3*, 1.

(103) Boden, A.; Boerner, B.; Kusch, P.; Firkowska, I.; Reich. S. Nanoplatelet Size to Control the Alignment and Thermal Conductivity in Copper/Graphite Composites. *Nano Lett.* **2014**, *14*, 3640.

(104) Guo, W.; Chen, G. Fabrication of graphene/epoxy resin composites with much enhanced thermal conductivity via ball milling technique. *App. Polym. Sci.* **2014**, *131*, 40565.

(105) Shtein, M.; Nadiv, R.; Buzaglo, M.; Kahil, K.; Regev, O. Thermally conductive graphene-polymer composites: Size, percolation, and synergy effects. *Chem. Mater.* **2015**, *27*, 2100.

(106) Shahil, K.M.F.; Balandin, A.A.; Graphene–Multilayer Graphene Nanocomposites as Highly Efficient Thermal Interface Materials. *Nano lett.* **2012**, *12*, 861.

(107) Li, Q.; Guo, Y.; Li, W.; Qiu, S.; Zhu, C.; Wei, X.; Chen, M.; Liu, C.; Liao, S.; Gong, Y.; Mishra, A. K.; Liu, L. Ultrahigh Thermal Conductivity of Assembled Aligned Multilayer Graphene/Epoxy Composite. *Chem. Mater.* **2014**, *26*, 4459.

(108) Zhang, Y.F.; Ren, Y.J.; Bai, S.L. Vertically Aligned Graphene Film/epoxy Composites as Heat Dissipating Materials. *Int. J. Heat Mass Transfer* **2018**, *118*, 510.

(109) Zhang, Y.F.; Han, D.; Zhao, Y.H.; Bai, S.L. High-performance thermal interface materials consisting of vertically aligned graphene film and polymer. *Carbon* **2016**, *109*, 552.

(110) Lian, G.; Tuan, C.C.; Li, L.; Jiao, S.; Wang, Q.; Moon, K.S.; Cui, D.; Wong, C. P. Vertically Aligned and Interconnected Graphene Networks for High Thermal Conductivity of Epoxy Composites with Ultralow Loading. *Chem. Mater.* **2016**, *28*, 6096.

(111) Alam, F.E.; Dai, W.; Yang, M.; Du, S.; Li, X.; Yu, J.; Jiang, N.; Lin, C.T. In situ formation of a cellular graphene framework in thermoplastic composites leading to superior thermal conductivity. *J. Mater. Chem. A* **2017**, *5*, 6164.

(112) Li, X.; Shao, L.; Song, N.; Shi, L.; Ding, P. Enhanced thermal-conductive and anti-dripping properties of polyamide composites by 3D graphene structures at low filler content. *Compos. Part:A-Appl. Sci. Manuf.* **2016**, *88*, 305.

(113) Meng, F.; Huang, F.; Guo, Y.; Chen, J.; Chen, X.; Hui, D.; He, P.; Zhou, X.; Zhou, Z. In Situ Intercalation Polymerization Approach to Polyamide-6/graphite Nanoflakes for Enhanced Thermal Conductivity. *Compos. Part B-Eng.* **2016**, *117*, 165.

(114) Jung, H.; Yu, S.; Bae, N. S.; Cho, S.M.; Kim, R. H.; Cho, S. H.; Hwang, I.; Jeong, B.; Ryu, J. S.; Hwang, J.; Hong, S. M.; Koo, C. M.; Park, C. High through-plane thermal conduction of graphene nanoflake filled polymer composites melt-processed in an L-shape kinked tube. *ACS Appl. Mater. Interfaces* **2015**, *7*, 15256.

(115) Yang, J.; Qi, G. Q.; Liu, Y.; Bao, R.Y.; Liu, Z.Y.; Yang, W.; Xie, B. H.; Yang, M.B. Hybrid graphene aerogels/phase change material composites: Thermal conductivity, shape-stabilization and light-to-thermal energy storage. *Carbon* **2016**, *100*, 693.

(116) Li, A.; Zhang, C.; Zhang, Y.F. RGO/TPU composite with a segregated structure as thermal interface material. *Compos. A Appl. Sci. Manuf.* **2017**, *101*, 108.

(117) Kumar, P.; Yu, S.; Shahzad, F.; Hong, S.M.; Kim, Y.H.; Koo, C.M. Ultrahigh electrically and thermally conductive self-aligned graphene/polymer composites using large-area reduced graphene oxides. *Carbon* **2016**, *101*, 120.

(118) Song, N.; Jiao, D.; Cui, S.; Hou, X.; Ding, P.; Shi, L. Highly Anisotropic Thermal Conductivity of Layer-by- Layer Assembled Nanofibrillated Cellulose/Graphene Nanosheets Hybrid Films for Thermal Management. *ACS Appl. Mater. Interfaces* **2017**, *9*, 2924.

(119) Goyal, V.; Balandin, A.A. Thermal Properties of the Hybrid Graphene-Metal Nano-Micro-Composites: Applications in Thermal Interface Materials. *App. Phys. Lett.* **2012**, *100*, 073113.

(120) Im, H.; Kim, J. Thermal Conductivity of a Graphene Oxide-Carbon Nanotube Hybrid/epoxy Composite *Carbon* **2012**, *50*, 5429.

(121) Parent, O.; Ilinca, A. Anti-icing and de-icing techniques for wind turbines: Critical review. *Cold Reg. Sci. Technol.* **2011**, *65*, 88.

(122) Kreder, M.J.; Alvarenga, J.; Kim, P.; Aizenberg, J. Design of Anti-Icing Surfaces: Smooth, Textured or Slippery. *Nat. Rev. Mater.* **2016**, *1*, 1.

(123) Lv, J.; Song, Y.; Jiang, L.; Wang, J. Bio-Inspired Strategies for Anti-Icing. *ACS Nano* **2014**, 8, 3152.

(124) Petrenko, V.F.; Sullivan, C.R.; Kozlyuk, V.; Petrenko, F.V.; Veerasamy, V. Electro- thermal De-icer (PETD). *Cold Reg. Sci. Technol.* **2011**, *65*, 70.

(125) Volman, V.; Zhu, Y.; Raji, A.R. O.; Genorio, B.; Lu, W.; Xiang, C.; Kittrell, C.; Tour, J.M. Radiofrequency Transparent , Electrically Conductive Graphene Nanoribbon Thin Films as De-icing Heating Layers. *Appl. Mater. Interfaces* **2014**, *6*, 298.

(126) Janas, D.; Koziol, K.K. A review of production methods of carbon nanotube and graphene thin films for electrothermal applications. *Nanoscale* **2014**, *6*, 3037.

(127) Raji, A.O.; Varadhachary, T.; Nan, K.; Wang, T.; Lin, J.; Ji, Y.; Genorio, B.; Zhu, Y.; Kittrell, C.; Tour, J.M. Composites of Graphene Nanoribbon Stacks and Epoxy for Joule Heating and Deicing of Surfaces. *Appl. Mater. Interfaces* **2016**, *8*, 3351.

(128) Chen, L.; Zhang, Y.; Wu, Q. Effect of Graphene Coating on the Heat Transfer Performance of a Composite Anti-/Deicing Component. *Coatings* **2017**, *7*, 158.

(129) Zhang, Q.; Yu, Y.; Yang, K.; Zhang, B.; Zhao, K.; Xiong, G.; Zhang, X. Mechanically robust and electrically conductive graphene-paper / glass- fibers / epoxy composites for stimuli-responsive sensors and Joule heating deicers. *Carbon* **2017**, *124*, 296.

(130) Bustillos, J.; Zhang, C.; Boesl, B.; Agarwal, A. Three – Dimensional Graphene Foam - Polymer Composite with Superior Deicing Efficiency and Strength. *ACS Appl. Mater. Interfaces* **2018**, *10*, 5022.

(131) Callow, J.A.; Callow, M.E. Trends in the development of environmentally friendly fouling-resistant marine coatings. *Nat. Comm.* **2011**, *2*, 244.

(132) Mates, J.E.; Bayer, I.S.; Palumbo, J.M.; Carroll, P.J.; Megaridis, C.M. Extremely stretchable and conductive water-repellent coatings for low-cost ultra-flexible electronics. *Nat. Comm.* **2015**, *6*, 8874.

(133) Feng, L.; Li, S.; Li, H.; Zhai, J.; Song, Y.; Jiang, L.; Zhu. D. Super-hydrophobic surface of aligned polyacrylonitrile nanofibers. Angew. Chem. Int. Ed. **2002**, *41*, 1221.

(134) Li, Y.; Huang, X.J.; Heo, S.H.; Li, C.C.; Choi, Y.K.; Cai, W.P.; Cho, S.O. Superhydrophobic bionic surfaces with hierarchical microsphere/SWCNT composite arrays. *Langmuir*, **2007**, *23*, 2169.

(135) Rafiee, J.; Rafiee, M. A.; Yu, Z.Z.; Koratkar, N. Superhydrophobic to Superhydrophilic Wetting Control in Graphene Films. *Adv. Mater.* **2010**, *22*, 2151.

(136) Zhang, X.; Wan, S.; Pu, J.; Wang, L.; Liu, X. Highly hydrophobic and adhesive performance of graphene films. *J. Mater. Chem.* **2011**, *21*, 12251.

(137) Dong, J.; Yao, Z.H.; Yang, T.Z.; Jiang, L.L.; Shen C.M. Control of Superhydrophilic and Superhydrophobic Graphene Interface. *Sci. Rep.* **2013**, *3*, 1733

(138) Wang, S.; Zhang, Y.; Abidi, N.; Cabrales, L. Wettability and Surface Free Energy of Graphene Films. *Langmuir*, **2009**, *25*, 11078.

(139) Xue, Y.; Liu, Y.; Lu, F.; Qu, J.; Chen, H.; Dai, L. Functionalization of Graphene Oxide with Polyhedral Oligomeric Silsesquioxane (POSS) for Multifunctional Applications. *J. Phys. Chem. Lett.* **2012**, *3*, 1607.

(140) Lee, J.S.; Yoon, J.C.; Jang, J.H. A route towards superhydrophobic graphene surfaces: surface-treated reduced graphene oxide spheres. *J. Mater. Chem. A*, **2013**, *1*, 7312.

(141) Zang, J.; Ryu, S.; Pugno, N.; Wang, Q.; Tu, Q.; Buehler, M.J.; Zhao, X. Multifunctionality and control of the crumpling and unfolding of large-area graphene. *Nat. Mater.* **2013**, *12*, 321.

(142) Chen, Z.; Dong, L.; Yang, D.; Lu, H. Superhydrophobic Graphene-Based Materials: Surface Construction and Functional Applications. *Adv. Mater.* **2013**, *25*, 5352.

(143) Nguyen, D.D.; Tai, N.H.; Lee, S.B.; Kuo, W.S. Superhydrophobic and superoleophilic properties of graphene-based sponges fabricated using a facile dip coating method. *Energy Environ. Sci.*, **2012**, *5*, 7908.

(144) Bi, H.; Xie, X.; Yin, K.; Zhou, Y.; Wan, S.; He, L.; Xu, F.; Banhart, F.; Sun, L.; Ruoff, R. S. Spongy Graphene as a Highly Efficient and Recyclable Sorbent for Oils and Organic Solvents. *Adv. Func. Mater.* **2012**, *22*, 4421.

(145) Singh, E.; Chen, Z.; Houshmand, F.; Ren, W.; Peles, Y.; Cheng, H.; Koratkar, N. Superhydrophobic Graphene Foams. *Small* **2013**, *9*, 75.

(146) Hu, H.; Zhao, Z.; Wan, W.; Gogotsi, Y.; Qiu, J. Polymer/Graphene Hybrid Aerogel with High Compressibility, Conductivity, and "Sticky" Superhydrophobicity. *ACS Appl. Mater. Interfaces* **2014**, *6*, 3242.

(147) Wang, P.; Yao, T.; Sun, B.; Fan, X.; Dong, S.; Bai, Y.; Shi, Y. A cost-effective method for preparing mechanically stable anti-corrosive superhydrophobic coating based on electrochemically exfoliated graphene. *Colloid Surf. A Physicochem. Eng. Asp.* **2017**, *513*, 396.

(148) Nine, M.J.; Cole, M.A.; Johnson, L.; Tran, D.N.H.; Losic, D. Robust Superhydrophobic Graphene-Based Composite Coatings with Self-Cleaning and Corrosion Barrier Properties. *ACS Appl. Mater. Interfaces* **2015**, *7*, 28482.

(149) Bharathidasan, T.; Narayanan, T.N.; Sathyanaryanan, S.; Sreejakumari, S.S. Above 170º water contact angle and oleophobicity of fluorinated graphene oxide based transparent polymeric film. *Carbon* **2015**, *84*, 207.

(150) Yang, Z.; Wang, L.; Sun, W.; Li, S.; Zhu, T.; Liu, W.; Liu, G. Superhydrophobic epoxy coating modified by fluorographene used for anti-corrosion and self-cleaning. *App. Surf. Sci.* **2017**, *401*, 146.

(151) Zhu, H.; Chen, D.; Li, N.; Xu, Q.; Li, H.; He, J.; Lu, J. Graphene Foam with Switchable Oil Wettability for Oil and Organic Solvents Recovery. *Adv. Funct. Mater.* **2015**, *25*, 597.

(152) Wang, Y.; Wang, L.; Yang, T.; Li, X.; Zang, X.; Zhu, M.; Wang, K.; Wu, D.; Zhu, H. Wearable and Highly Sensitive Graphene Strain Sensors for Human Motion Monitoring. *Adv. Funct. Mater*. **2014**, 24, 4666.

(153) Lin, Y.; Dong, X.; Liu, S.; Chen, S.; Wei, Y.; Liu, L. Graphene − Elastomer Composites with Segregated Nanostructured Network for Liquid and Strain Sensing Application. *ACS Appl. Mater. Interfaces* **2016**, *8*, 24143.

(154) Kuang, J.; Liu, L.; Gao, Y.; Zhou, D.; Chen, Z.; Han, B.; Zhang, Z. A hierarchically structured graphene foam and its potential as a large-scale strain-gauge sensor. *Nanoscale* **2013**, *5*, 12171.

(155) Liu, H.; Dong, M.; Huang, W.; Gao, J.; Dai, K.; Guo, J.; Zheng, G.; Lou, C.; Shen, C.; Guo, Z. Lightweight conductive graphene/thermoplastic polyurethane foams with ultrahigh compressibility for piezoresistive sensing. *J. Mater. Chem. C.* **2017**, *5*, 73.

(156) Boland, C.S.; Khan, U.; Backes, C.; O'Meill, A.; mcCauley, J.; Duane, S.; Shanker, R.; Liu, Y.; Jurewicz, I.; Dalton, A.B.; Coleman, J. N. Sensitive, High-Strain, High-Rate Bodily Motion Sensors Based on Graphene-Rubber Composites. *ACS Nano* **2014**, *8*, 8819.

(157) Lin, Y.; Dong, X.; Liu, S.; Chen, S.; Wei, Y.; Liu, L. Graphene − Elastomer Composites with Segregated nanostructured Network for Liquid and Strain Sensing Application. *ACS Appl. Mater. Interfaces* **2016**, *8*, 24143.

(158) Shao, Y.; Wang, J.; Wu, H.; Liu, J.; Aksay, I.A.; Lin, Y.; Graphene Based Electrochemical Sensors and Biosensors: A Review. *Electroanal.* **2010**, *22*, 1027.

(159) Huanh, X.; Leng, T.; Georgiou, T.; Abraham, J.; Nair, R.R.; Novoselov, K.S.; Hu, Z. Graphene Oxide Dielectric Permittivity at GHz and Its Applications for Wireless Humidity Sensing. *Sci. Rep.* **2018**, *8*, 43.

(160) Watthanawisuth, N.; Maturos, T.; Sappat, A.; Tuantranont, A. The IoT Wearable Stretch Sensor Using 3D-Graphene Foam. *IEEE Sens. J.* **2015**, *978*, 4799.

(161) Wicklein, B.; Kocjan, A.; Salazar-Alvarez, G.; Camino, G.; Antonietti, M.; Bergstrom, L. Thermally insulating and fire-retardant lightweight anisotropic foams based on nanocellulose and graphene oxide. *Nat. Nanotechnol.* **2015**, *10*, 277.

(162) Huang, G.; Gao, J.; Wang, X.; Liang, H.; Ge, C. How can graphene reduce the flammability of polymer nanocomposites? *Mater. Lett.* **2012**, *66*, 187.

(163) Higginbotham, A.L.; Lomeda, J.R.; Morgan, A.B.; Tour, J.M. Graphite oxide flame-retardant polymer nanocomposites. *ACS Appl. Mater. Interfaces* **2009**, *1*, 2256.

(164) Shi, Y.; Li, L.J. Chemically modified graphene: Flame retardant or fuel for combustion? *J. Mater. Chem.* **2011**, *21*, 3277.

(165) Liu, S.; Yan, H.; Fang, Z.; Wang, H. Effect of graphene nanosheets on morphology, thermal stability and flame retardancy of epoxy resin. *Compos. Sci. Technol.* **2014**, *90*, 40.

(166) Zhou, K.; Gui, Z.; Hu, Y. The influence of graphene based smoke suppression agents on reduced fire hazards of polystyrene composites. *Compos Part A Appl Sci Manuf.* **2016**, *80*, 217.

(167) Jeon, I.Y.; Shin, S.H.; Choi, H.J.; Yu, S.Y.; Jung, S.M.; Baek, J.B. Heavily aluminated graphene nanoplatelets as an efficient flame retardant. *Carbon* **2017**, *116*, 77.

(168) Zhou, K.; Gui, Z.; Hu, Y.; Jiang, S.; Tang, G. The influence of cobalt oxide-graphene hybrids on thermal degradation, fire hazards and mechanical properties of thermoplastic polyurethane composites. *Compos Part A Appl Sci Manuf.* **2016**, *88*, 10.

(169) Han, Y.; Wang, T.; Gao, X.; Li, T.; Zhang, Q. Preparation of thermally reduced graphene oxide and the influence of its reduction temperature on the thermal, mechanical, flame retardant performances of PS nanocomposites. *Compos Part A Appl Sci Manuf.* **2016**, *84*, 336.

(170) Liu, S.; Fang, Z.; Yan, H.; Chevali, V.S.; Wang, H. Synergistic flame retardancy effect of graphene nanosheets and traditional retardants on epoxy resin. *Compos Part A Appl Sci Manuf.* **2016**, *89*, 26.

(171) Zhang, Z.; Yuan, L.; Guan, Q.; Liang, G.; Gu, A. Synergistically building flame retarding thermosetting composites with high toughness and thermal stability through unique phosphorus and silicone hybridized graphene oxide. *Compos Part A Appl Sci Manuf.* **2017**, *98*, 174.